Classical and quantum nonlinear localized excitations in discrete systems

FR Romero,* JFR Archilla, F Palmero, B Sánchez-Rey, A Álvarez, J Cuevas, and JM Romero

Grupo de Física No Lineal. Departamento de Física atómica,
molecular y nuclear y Departamento de Física Aplicada I. Universidad
de Sevilla. Avda. Reina Mercedes, s/n. 41012-Sevilla (Spain)

(Dated: April 10, 2005)

Discrete breathers, or intrinsic localized modes, are spatially localized, time–periodic, nonlinear excitations that can exist and propagate in systems of coupled dynamical units. Recently, some experiments show the sighting of a form of discrete breather that exist at the atomic scale in a magnetic solid. Other observations of breathers refer to systems such as Josephson–junction arrays, photonic crystals and optical-switching waveguide arrays. All these observations underscore their importance in physical phenomena at all scales. The authors review some of their latest theoretical contributions in the field of classical and quantum breathers, with possible applications to these widely different physical systems and to many other such as DNA, proteins, quantum dots, quantum computing, etc.

I. INTRODUCTION

Nonlinear physics of discrete systems has attained an enormous development in the previous years. A landmark is the prove of the existence of spatially localized, time–periodics oscillations in discrete nonlinear systems, by MacKay and Aubry [46]. They are now termed discrete breathers (DB), nonlinear localized excitations, or intrinsic localized modes, and ever since there are many experimental data and theoretical results published about these important new phenomenon in physics. They appear in lattices of oscillators interacting through nonlinear forces. The central class of system for which the concept of DB was developed is classical, autonomous spatially discrete Hamiltonian or reversible systems. A type of systems of this class is called Klein–Gordon lattices. They are Hamiltonian systems consisting of one degree of freedom anharmonic Hamiltonian oscillators coupled weakly in a lattice, that is, the frequency of oscillation of each oscillator varies non–trivially with the amplitude. Most studies on breathers have been done utilizing this type of models, with applications to biomolecules, such as DNA, solids, etc. Other classes of systems where breathers occur are: autonomous forced damped systems, and time–periodically forced systems. Considering applications to molecular crystals, quantum effects must be taken into account and the concept of quantum discrete breather should be developed. This review summarize some of the latest theoretical contributions in the field of localized nonlinear excitations carried out by the Nonlinear Physics Group of the Sevilla University. The structure of this work has the following scheme:

- Section II: Breathers in Klein–Gordon lattices with competing short and long–range interactions

  - A: DNA model with dipole–dipole coupling
  - B: Numerical methods for obtaining breathers and determining their stability
  - C: Bifurcations

- Section III: Moving breathers in homogeneous DNA chains

  - A: Moving breathers in DNA chains without curvature
  - B: Moving breathers in bent DNA chains
  - C: Parameters values of DNA

- Section IV: Interaction of moving breathers with mass impurities

---

*Electronic address: romero@us.es

II. BREATHERS IN KLEIN–GORDON LATTICES WITH COMPETING SHORT AND LONG–RANGE INTERACTIONS

Most of the studies about breathers in Klein–Gordon lattices refer to models which include only short–range interacting forces between the oscillators. This section reviews some of the results relative to breathers solutions in Klein–Gordon chains which include also long–range interactions.

A one–dimensional Klein–Gordon lattice is a chain of identical oscillators with an on–site potential V, each one of them coupled with its nearest neighbours through a parameter $C \ll 1$. The Hamiltonian of a chain of N oscillators is:

$$H = \sum_{n=1}^{N} \left(\frac{1}{2}\dot{u}_n^2 + V(u_n) + \frac{1}{2}C(u_n - u_{n-1})^2 \right),$$ (1)

where u_n represents the coordinates of the oscillators referred to their equilibrium positions, and $V(u_n)$ represents the on–site potential.

In addition to the short–range interaction coupling, other types of forces can also exist. For example, if each oscillator has an intrinsic dipole moment, there exist also long–range forces due to the dipole–dipole coupling, and consequently the Hamiltonian must be modified. The existence of these two competing forces could alter substantially the properties of the breathers solutions. The study is presented in the next subsections, selecting a DNA model which has also into account the existence of dipole–dipole coupling.

A. DNA model with dipole–dipole coupling

In DNA there exists different kinds of interactions between the main atomic groups. One of them is the stacking interaction between neighbour bases along the DNA axis, these are short–range forces which stabilize the DNA structure and hold one base over the next one forming a stack of bases. There exist also long–range forces, due to the finite dipole moments of the hydrogen bonds within the nucleotides [35, 51]. The dipole–dipole interactions between different base pairs become critical when the geometry of the double strand of DNA is taken into account, as the distance between base pairs and, therefore, the intensity of the coupling between them, depends on the shape of the molecule [5, 6, 23].

The Peyrard-Bishop DNA model [53] was initially introduced considering only the stacking interactions between base pairs. It can be modified by adding an energy term that takes into account the dipole–dipole forces. The Hamiltonian can be written as:

$$H = \sum_{n=1}^{N} \left(\frac{1}{2}m\dot{u}_n^2 + V(u_n) + \frac{1}{2}C(u_{n+1} - u_n)^2 + \frac{1}{2}\sum_{p \neq n} \frac{J}{|p|} u_{n+p} u_n \right).$$ (2)

The term $\frac{1}{2}m\dot{u}_n^2$ represents the kinetic energy of the nucleotide of mass m at the nth site of the chain, and u_n is the variable representing the transverse stretching of the hydrogen bond connecting the bases. The on–site potential is the Morse potential, i.e., $D(e^{-bu_n} - 1)^2$, represents the interaction energy due to the hydrogen bonds within the base

pairs, where D is the well depth and represents the dissociation energy of a base pair, and b^{-1} is related to the width of the well. The stacking energy is $\frac{1}{2}C(u_{n+1} - u_n)^2$, where C is the stacking coupling constant [53] . The last term of the Hamiltonian is the long-range dipole–dipole interaction term, where $J = q^2/4\pi\varepsilon_0 d^3$ is the dipole long-range interaction coupling constant [21], with q being the charge transfer due to the formation of the hydrogen bonds, and d the distance between base pairs, which is supposed to be constant. It is possible to consider $D = 1/2$, $b = 1$, $m = 1$ without loss of generality.

B. Numerical methods for obtaining breathers and determining their stability

A static breather (SB) can be obtained by solving the full dynamical equations, which can be obtained applying Hamilton's equations to (2). This aim can be achieved using common methods based on the anticontinuous limit [8, 46, 47, 48]. The implementation of these methods basically consists in calculating the orbit of an isolated oscillator at fixed frequency $\omega_{\rm b}$, and using this solution as a seed to solve the complete dynamical equations by means of a Newton–Raphson continuation method. A SB can be obtained for a given values of the dipole–dipole coupling parameter, J, and the stacking coupling parameter, C. This solution can be continued by varying C and maintaining J constant or vice versa.

The linear stability of a breather can be studied by performing a Floquet analysis [10]. To this end, it is necessary to consider the evolution of a perturbation ξ through the dynamical equations:

$$\ddot{\xi}_n + V''(u_n)\xi_n + C(2\xi_n - \xi_{n+1} - \xi_{n-1}) + \sum_{p \neq n} \frac{J}{p}\xi_{n+p} = 0. \tag{3}$$

The functions $\Omega(0) \equiv (\{\xi_n(0)\}, \{\dot{\xi}_n(0)\})$ must be integrated until $t = T$, giving $\Omega(T) \equiv (\{\xi_n(T)\}, \{\dot{\xi}_n(T)\})$. There exists a matrix of dimension $2N$ called the *monodromy*, which is defined by $\Omega(T) = \mathcal{M}\Omega(0)$.

The spectrum of this matrix has the following property: if λ is an eigenvalue, then λ^*, $1/\lambda$ and $1/\lambda^*$ are also eigenvalues. Therefore, stability implies that all the eigenvalues have modulus unity [20].

The procedure of continuation of SBs can be done as long as an integer multiple of their frequency does not resonate with any of the frequencies of the linear modes (or phonons). This resonance provides an analytical expression for the upper boundary delimiting the existence of SBs: $C = (\omega_{\rm b}/\omega_{\rm o})^2 - 1/4 + 3\zeta(3)J/8$.

C. Bifurcations

The study of the bifurcation loci of SBs is interesting for three different reasons: a) It gives the range of existence of the SBs; b) It gives the regions in the parameter space where the breathers are stable (and, therefore, physically observable in real systems) or unstable; c) Finally, but of paramount importance, it gives the values of the parameters where the breathers are movable.

Two types of bifurcations appear as C and J are varying: 1) Stability bifurcations: they occur when a breather changes its stability. The existence of this type of bifurcation is a necessary condition for the existence of movable breathers (see Section III). 2) Breather extinctions: they occur when a breather is not continuable any longer.

When only stacking interaction is considered, only stability bifurcations occur and moving breathers are possible. However, with only dipole-dipole interactions there are no stability bifurcations and, therefore, moving breathers do not exist.

When both interactions exist simultaneously, the analysis of 1-site (site-centered) and 2-site (bond-centered) breathers, permits to establish the following staments: A) 1–site breathers can be moved only for $J < J_{c1}$. B) 2–site breathers are movable for $J < J_{c2}$ being $J_{c2} > J_{c1}$. They are also movable for $J \in [J_{c2}, J_o)$. Therefore, J_o establishes the maximum value of J (and also the minimum value of C) for which breathers can be movable, i.e., *there are no moving breathers for $C < J_o$ and for $J > J_o$*. This is the reason why J_o is called the *mobility limit* [21].

The bifurcation loci for the stability bifurcations are shown in Fig. 1(a). Also, in Fig. 1(b) the dependence of the mobility limit with respect to the breather frequency is shown. This curve fits very well to the relation $J_o = A\omega_{\rm b}^r$, where A=0.1921 ± 0.0002 and r=2.377 ± 0.005.

III.   MOVING BREATHERS IN HOMOGENEOUS DNA CHAINS

This section is dedicated to the study of travelling breathers, or moving breathers, in DNA chains described by the Peyrard–Bishop modified model. The first subsection presents this study for straight line DNA chains, or chains
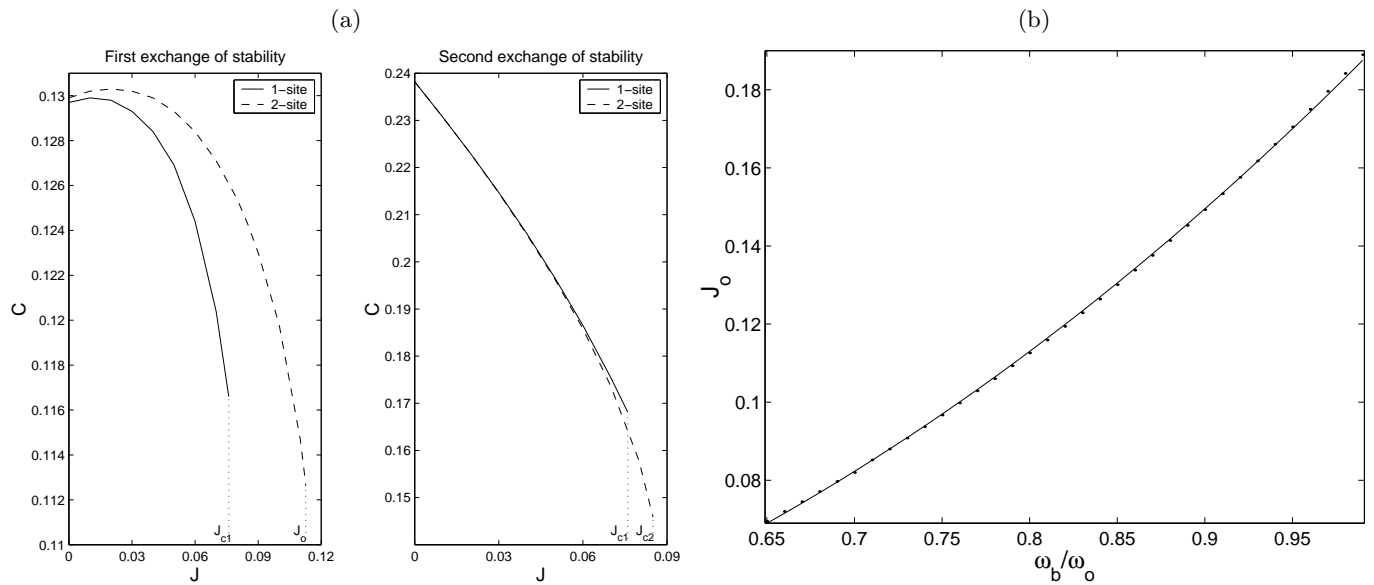
FIG. 1: (a) Bifurcation loci for the first and the second exchange of stability in 1-site and 2-site breathers. The values corresponding to $\omega_b = 0.8$ are: $J_{c1} = 0.076$, $J_{c2} = 0.085$, $J_o = 0.11263$. (b) Dependence of J_o with respect to the breather frequency.

without curvature. The next subsection considers DNA chains which have been bent and adapted to a parabola.

A. Moving breathers in DNA chains without curvature

Contrary to static breathers, moving breathers are not exact solutions of the dynamical equations of the model and they have a finite life due to the effects of phonon radiation. A moving breather is obtained by 'kicking' a static breather, i.e., perturbing its velocity components. However, not all breathers can be moved, and not every kick can move a breather. Therefore, it is important to know the conditions that a breather must fulfill in order to be movable and what the characteristics of the perturbations are. As indicated in [11, 17, 19], the following steps must be performed in order to obtain a moving breather: 1) To look for the existence of the two complementary stability bifurcations for the 1–site breather and the 2–site breather. Their bifurcation loci must have a region where they are fairly close. The static breather that can be moved should be obtained for values of the parameters close enough to these bifurcation loci. However, as shown in [21] it is only necessary that the static breather is "quasi-stable", i.e., not very stable or not very unstable; 2) To perturb the breather with the velocity components of the marginal mode at the neighbouring bifurcation. Time evolution of a moving breather is shown in Fig. 2.

An useful concept used for describing the breather dynamics is its effective mass [11, 17]. It is a measure of the breather inertia to external forces. The breather velocity must be perturbed in a direction colinear to the *marginal mode* in order to obtain moving breathers. This mode is the responsible for the stability bifurcation. If the normalized marginal mode is $\mathbf{V}$, the perturbation added to the breather velocities, which are zero at $t = 0$, is given by $\lambda\mathbf{V}$, and λ is the magnitude of the perturbation. Thus, the kinetic energy added to the breather by the initial kick is $1/2\lambda^2$. It is found that the resulting translational velocity of the breather, v, is proportional to λ. Then, the concept of effective mass can be defined through the relation $m^*v^2/2 = \lambda^2/2$. Therefore, $m^* = (\lambda/v)^2$. Consequently, moving breathers can be considered as a quasi-particle with mass m^*. The effective mass is a quantitative measure of the breather mobility. Larger mass indicates smaller mobility.

Numerical studies show that, for high values of the dipole–dipole coupling, the predicted range of existence of moving breathers decreases and, in some cases, it is impossible for the breather to be moved even in the neighbourhood of the stability bifurcations. Another important result is that the dipole–dipole interaction affects to the mobility of the breathers. The study of the dependence of the breather effective mass, shows that the mobility decreases when the intensity of the dipole–dipole coupling increases (see Fig. 3).
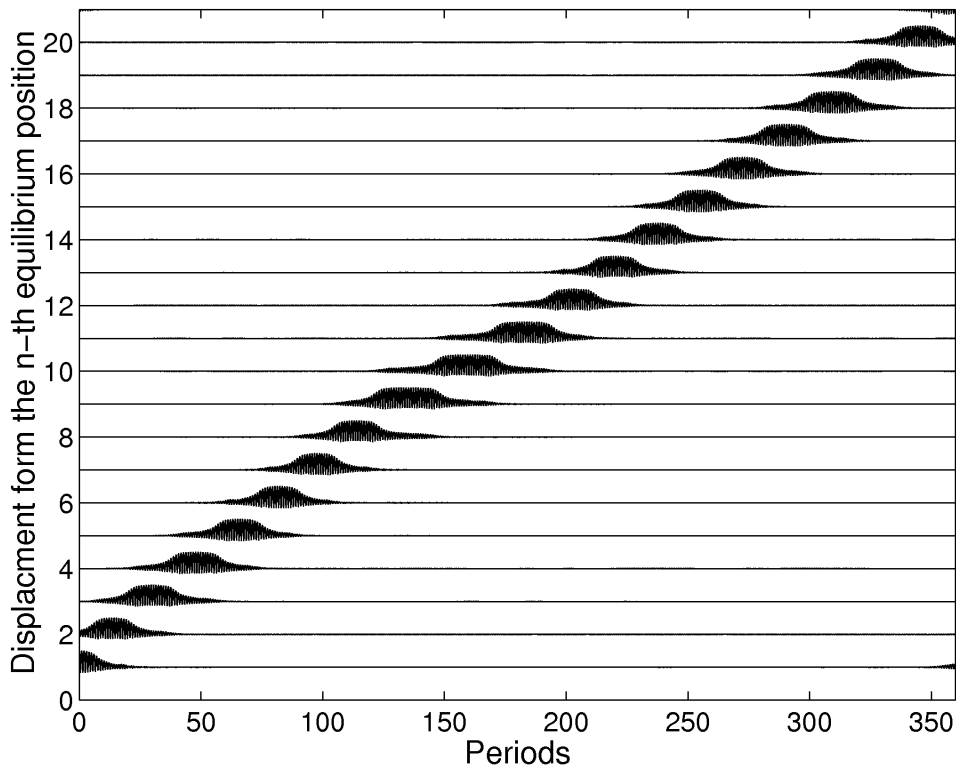
FIG. 2: Evolution of a moving breather for $C = 0.1244$, $J = 0.06$ and an initial 'kick' $\lambda = 0.10$. The breather involves basically three sites that oscillate in phase.

B. Moving breathers in bent DNA chains

Suppose a DNA chain lying in a plane which has been bent and adapted to a parabola of curvature κ (that is, the location of the n-th base pair is determined by the equation $y_n = \kappa x_n^2/2$) [5]. All the dipole moments are perpendicular to the plane and parallel among them. Thus, the modified Hamiltonian of Eq. (2) is:

$$H = \sum_{n=1}^{N} \left(\frac{1}{2}m\dot{u}_n^2 + V(u_n) + \frac{1}{2}C(u_{n+1} - u_n)^2 + \frac{1}{2}\sum_{p \neq n} \frac{J}{|\vec{r}_n - \vec{r}_p|^3} u_{n+p} u_n \right), \tag{4}$$

where $\vec{r}_n = (x_n, y_n)$, and it is assumed that the chain is inextensible, so that the distance between neighbouring sites remains constant: $|\vec{r}_n - \vec{r}_{n+1}| \equiv d$.

Fig. 4(a) illustrates the evolution of the energy centre [21] of a moving breather in a bent chain. If the added kinetic energy, $E = \lambda^2/2$, is smaller than a critical value E_c, the breather rebounds, but, if $E > E_c$, the breather passes through the bending point. Fig. 4(b) shows that the critical energy increases monotonically with the curvature.

Chain bending acts as a hindrance for the movement of breathers. This hindrance resembles to the experimented by a particle moving in a potential barrier. In this case, breather can be consider as a quasi-particle and this barrier can be calculated by finding the points where breathers rebound, i.e., the turning points for different values of E. Furthermore, if the breather has a constant effective mass m^*, this potential barrier can be obtained using the expression:

$$E_b(x) = \frac{1}{2}\lambda^2[1 - (v(x)/v_o)^2], \tag{5}$$

where $v(x)$ is the translational velocity and v_o is its value at $t = 0$. Fig. 5 show that there exists a good agreement between the barriers calculated using both methods for a given value of κ. The barrier calculated by the second method exhibits an irregular shape, whose origin lies in the non-uniform behaviour of the translational velocity due
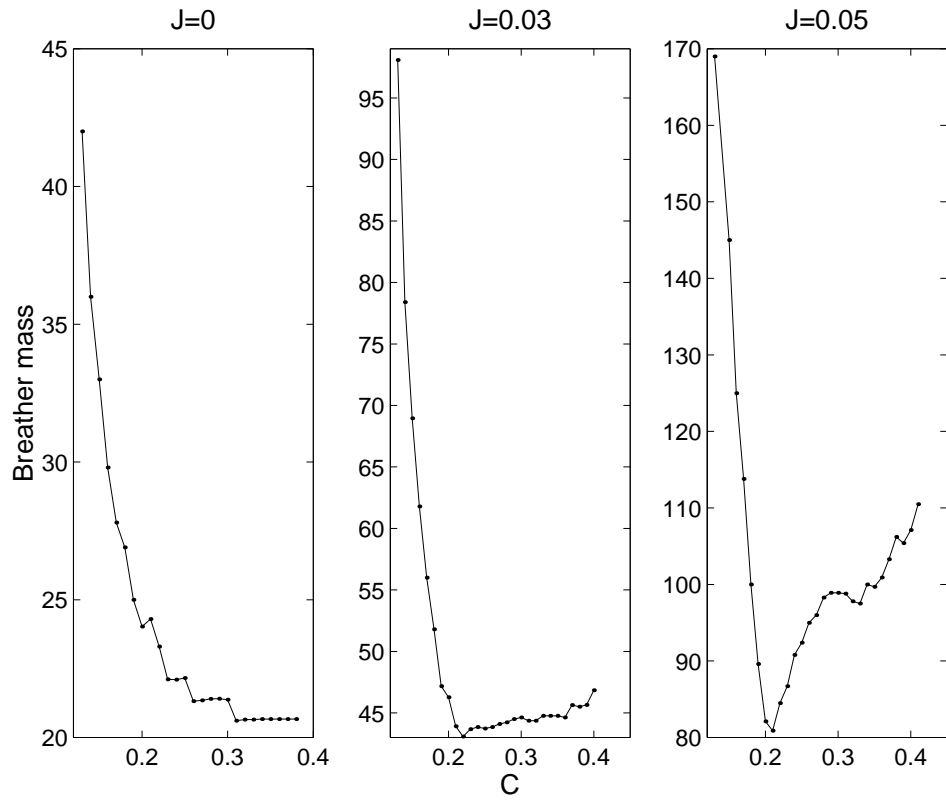
FIG. 3: Breather mass versus stacking coupling parameter C for dipole–dipole coupling parameter $J = 0$ (left), $J = 0.03$ (center) and $J = 0.05$ (right). Note that the maximum value of the mass occurs at the first bifurcation, and that the breather mass for $J = 0.05$ is always greater than the mass for $J = 0$. Note also the different scales at the Y-axis.
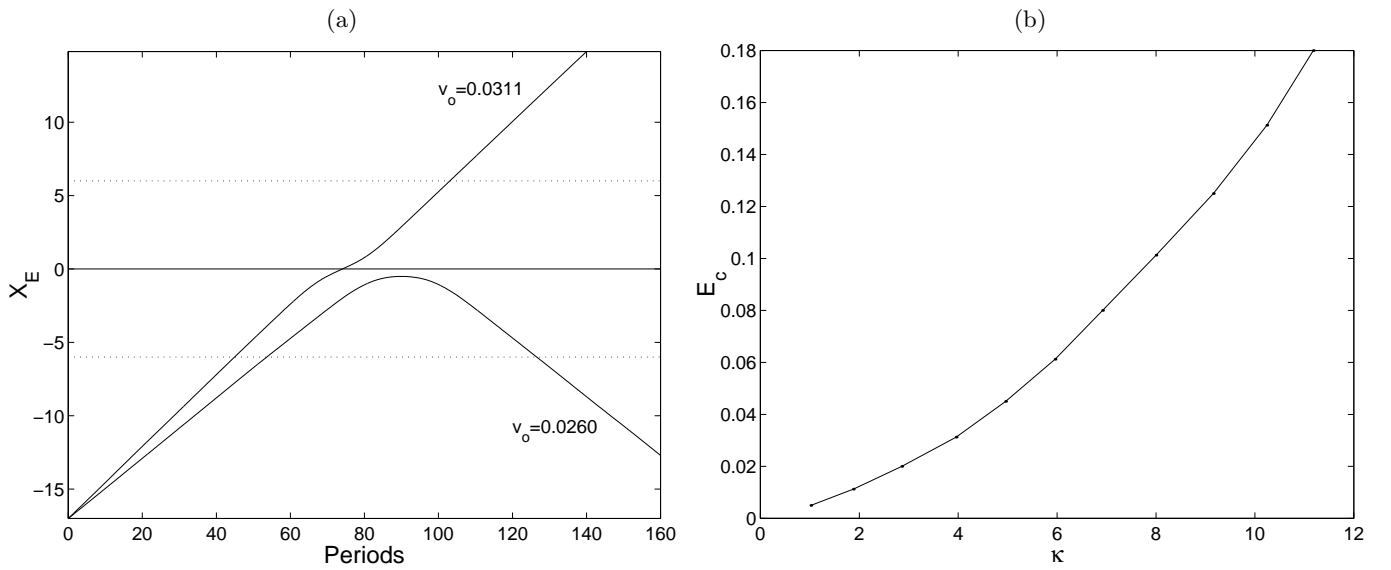

FIG. 4: (a)Evolution of the breather energy centre (X_E) for two different initial velocities. The curvature is $\kappa = 2$. (b) Critical kinetic energy E_c versus curvature κ.
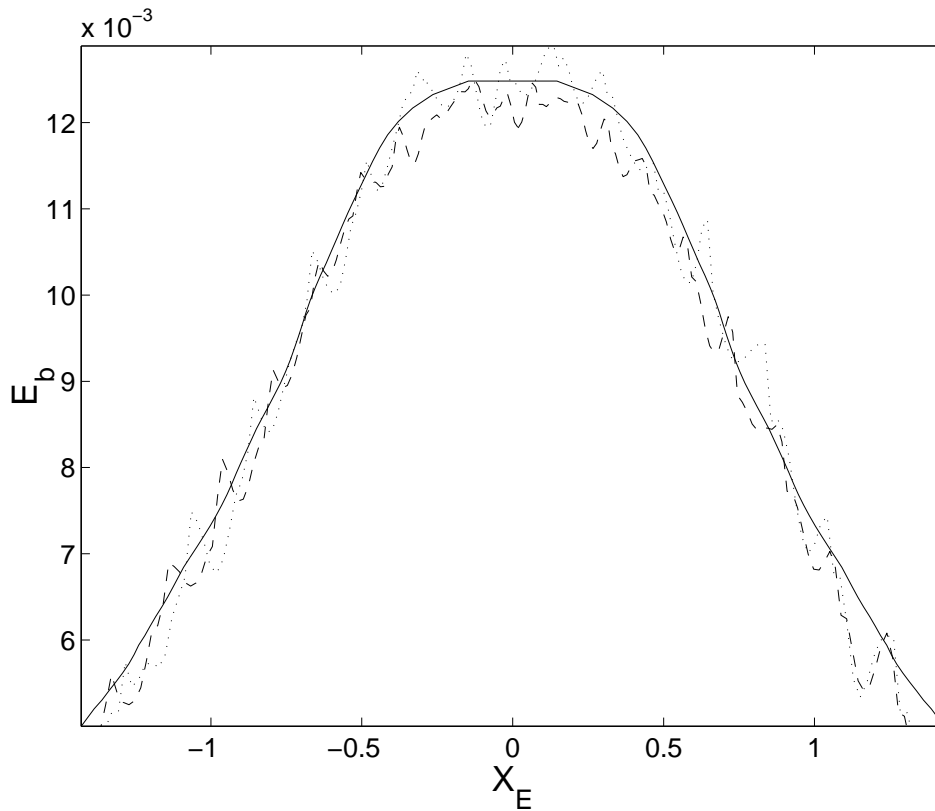
FIG. 5: Potential barrier calculated finding the turning points (solid line) and using Eq. (5) for $E = 0.0162$ (dashed lined) and $E = 0.0200$ (dotted line). The curvature is $\kappa = 2$ and the critical energy is $E_c \approx 0.0126$. The zero value of the energy centre (X_E) represents to the bending point.

to the discreteness of the system [19]. This result confirms that, in this case, a moving breather behaves as a particle of constant effective mass m^*.

It is worth remarking that a similar study has been performed in bent alpha–helix proteins [7].

C.   Parameters values of DNA

The results presented are valid for all chains with both short range and long range interactions given by equations (2) and (4). When they model a DNA chain, the following parameter values should be used [25]: $D = 0.04$ eV, $b = 4.45$ Å^{-1}, $d = 3.4$ Å, $J = 0.0031$ eV/Å^2, $C = (0.01, 10)$ eV/Å^2, $m = 300$ amu and the time unit is 0.88 ps. For this set of values, the minimal kinetic energy for a moving breather to cross the bending point is small, and, in consequence, it seems plausible that most MBs will have enough energy to pass through bending points, although the ones with low energy will be reflected.

IV.   INTERACTION OF MOVING BREATHERS WITH MASS IMPURITIES

Sometimes a chain can have a single point inhomogeneity, that is, the chain is homogeneous except at a single site where,for example, an impurity or a different type of particle is located. Moving breathers can be generated far apart the impurity and be launched towards it. This section presents some results relative to the effects of the collisions of moving breathers with an impurity in a Klein–Gordon chain.
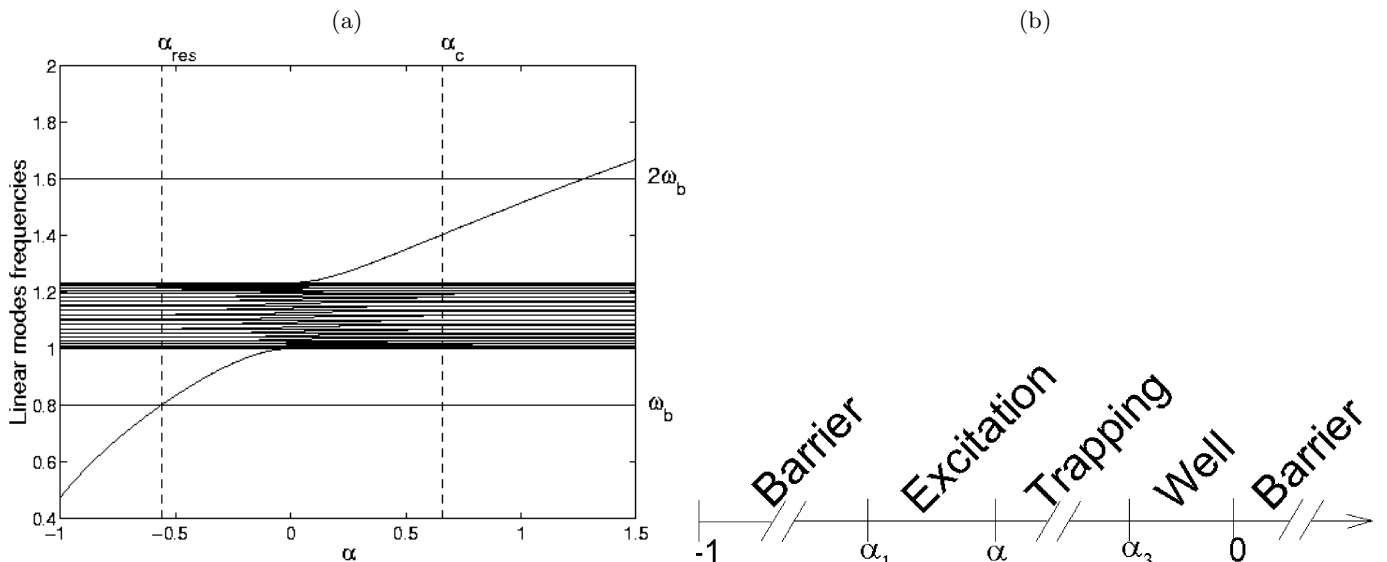
FIG. 6: (a) Frequencies of the linear modes versus the parameter α. At $\alpha = \alpha_{res}$ and $\alpha = \alpha_c$, two different bifurcations occur, being the first one due to the resonance between the impurity mode and the breather. (b) Different regimes in the interaction of a moving breather with an impurity.

Consider a Klein–Gordon chain with nearest neighbours attractive interactions, with Hamiltonian given by:

$$H = \sum_{n=1}^{N} \left(\frac{1}{2} \dot{u}_n^2 + V_n(u_n) + \frac{1}{2} C(u_n - u_{n-1})^2 \right), \tag{6}$$

where $V_n(u_n) = D_n(e^{-u_n} - 1)^2$ is a substrate potential at the n-th site. The inhomogeneity is introduced assuming a different well depth at a single site, i.e., $D_n = D_o(1 + \alpha \delta_{n,0})$, where $\alpha \in [-1, \infty)$ is a parameter which tunes the magnitude of the inhomogeneity. The particle located at $n = 0$ is an impurity.

The dynamical equations can be linearized if the amplitudes of the oscillations are small enough. These equations have $N - 1$ non-localized solutions (*linear extended modes*) and one localized solution, (*linear impurity mode*). Their frequencies, ω_E and ω_L, are given, respectively, by:

$$\omega(q, \alpha) = \sqrt{\omega_o^2 + 4C \sin^2 \frac{q(\alpha)}{2}}, \quad \omega_L^2 = \omega_o^2 + 2C + \text{sign}(\alpha)\sqrt{\alpha^2 \omega_o^4 + 4C^2}, \tag{7}$$

where $q \in (0, \pi]$ if $\alpha < 0$ and $q \in [0, \pi)$ if $\alpha > 0$. Fig. 6(a) shows the dependence on α.

Numerical simulations show that, depending of the critical values of the parameter α, there exist four different regimes in the moving breather–impurity interaction [24]: 1) *Barrier*. The impurity acts as a potential barrier. It occurs either with $\alpha > 0$ or $\alpha \in (-1, \alpha_1)$ with $\alpha_1 < 0$. If $\alpha \gtrsim 0$, the breather can pass through the impurity provided the translational velocity is high enough [23]. *Excitation*. The impurity is excited and the breather is reflected. This case appears for $\alpha \in (\alpha_1, \alpha_2)$, an example can be seen in Fig. 7(a). 3) *Trapping*. The breather is trapped by the impurity. It occurs in the interval $\alpha \in (\alpha_2, \alpha_3)$. When the moving breather is close to the impurity, it becomes trapped while its center oscillates between the neighbouring sites, as Fig. 7(b) shows. 4) *Well*. The impurity acts as a potential well. It occurs for $\alpha \in (\alpha_3, 0)$ and consists of an acceleration of the breather as it approaches to the impurity, and a deceleration after the breather has passed through the impurity.

It is observed that the breather bifurcates with the zero solution at $\alpha = \alpha_{res}$. That is, for α smaller than this value, no impurity breather exists. At $\alpha = \alpha_{res}$, the frequency of the impurity mode coincides with the moving breather frequency, i.e., in (7), $\omega_L = \omega_b$.

The scenario for the trapped breathers when $\alpha < 0$ is the following: the impurity mode has $q = 0$, and also all the particles of the impurity breather vibrate in phase; this vibration pattern indicates that the impurity breather bifurcates from the impurity mode and it will be the only localized mode that exists when the impurity is excited for $\alpha > \alpha_{res}$. Thus, when the moving breather reaches the impurity, it can excite the impurity mode. For $\alpha < \alpha_{res}$, the moving breather is always reflected. In addition, the impurity breather does not exist. Therefore, there might be a connection between both facts, i.e., the existence of the impurity breather seems to be a necessary condition in order
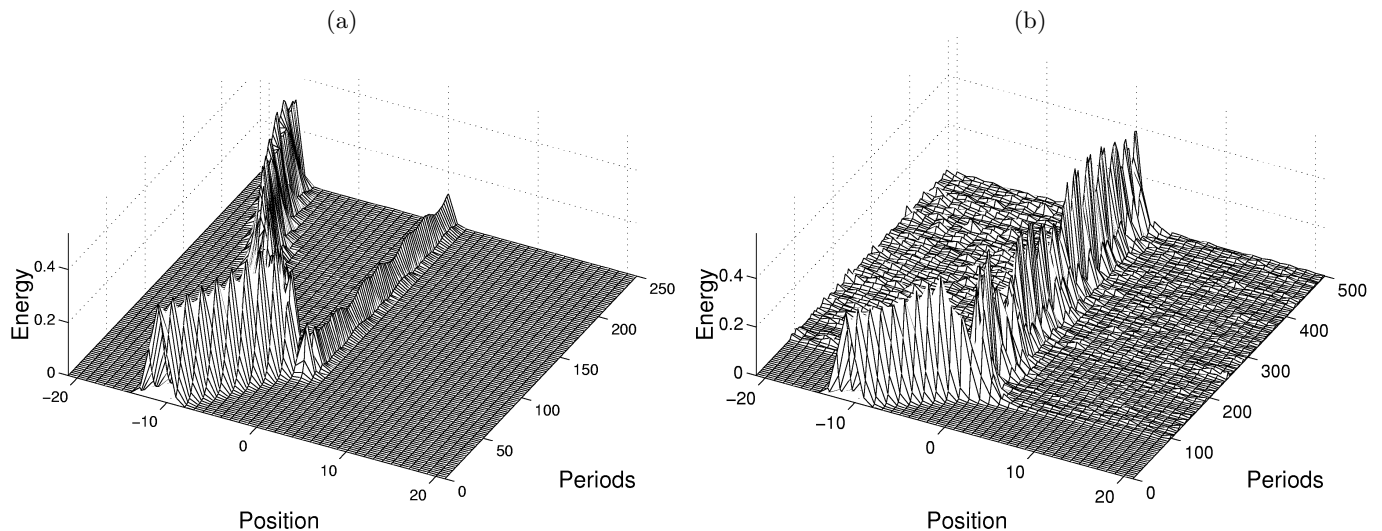
(a)

(b)

FIG. 7: (a) Interaction of a breather with an impurity for $\alpha = -0.52$, which corresponds to the impurity excitation case. (b) Evolution of the moving breather for $\alpha = -0.3$, which corresponds to the trapping case. The moving breather becomes trapped by the impurity; afterwards, the breather emits phonon radiation and its energy centre oscillates between the sites adjacent to the impurity.

to obtain a trapped breather. If $\alpha > 0$, the impurity mode has $q = \pi$ but the impurity breather's sites vibrate again in phase, that is, the impurity breather does not bifurcate from the impurity mode. There are two different localized excitations: the tails of the (linear) impurity mode and the impurity breather. Thus, if the moving breather reaches the impurity site, it will excite these localized excitations. Therefore, we conjecture that the existence of both linear localized entities at the same time may be the reason why the impurity is unable to trap the breather when $\alpha > 0$.

All these facts allows the formulation of the following trapping hypothesis: *The existence of an impurity breather for a given value of α is a necessary condition for the existence of trapped breathers. However, if there exists an impurity mode with a vibration pattern different from the impurity breather one's, the trapped breather does not to exist.*

V. INTERACTION OF MOVING BREATHERS WITH VACANCIES

Another type of local inhomogeneity that can exists in a homogeneous chain is a vacancy, that is, the absence of a particle at a single site. A moving breather can be launched towards the vacancy and the effects of the collision should be analyzed.

Consider a Hamiltonian Frenkel–Kontorova model with an anharmonic interaction potential [16]:

$$H = \sum_n \frac{1}{2}\dot{x}_n^2 + \frac{1}{4\pi^2}[1 - \cos(2\pi x)] + C\frac{1}{2b^2}[\exp(-b(x_{n+1} - x_n - 1)) - 1]^2, \tag{8}$$

where $\{x_n\}$ are the absolute coordinates of the particles. The choice of a periodic potential makes easy to represent a vacancy. Thus, if the vacancy is located at site n_v (see Fig. 8), the displacements of the particles with respect to their equilibrium positions are:

$$\begin{cases} u_n = x_n - nL & n < n_v \\ u_n = x_n - (n+1)L & n > n_v. \end{cases} \tag{9}$$

It is possible to generate a moving breather travelling towards the vacancy at the site n_v, and simulate the collision with this type of point inhomogeneity.

The initial perturbation, $\{\mathbf{V}_n\}$ has been chosen as $\mathbf{V} = \lambda(\ldots, 0, -1/\sqrt{2}, 0, 1/\sqrt{2}, 0, \ldots)$, where the nonzero values correspond to the neighboring sites of the initial center of the breather.
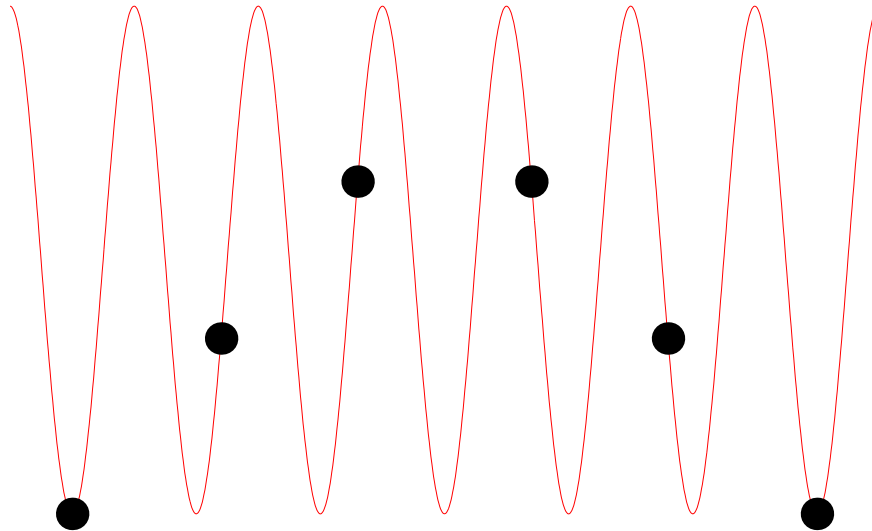
FIG. 8: Scheme of the Frenkel–Kontorova model with sine-Gordon on–site potential, with full circles representing to the particles.

When a moving breather reaches the site occupied by the particle adjacent to the vacancy, i.e., the location $n_v - 1$, the particle can jump to the vacancy site or remain at rest. If the former takes place, the vacancy moves backwards. However, if the interaction potential is wide enough, the particle at the $n_v + 1$ site, can feel the effect of the moving breather at the $n_v - 1$ site and it can also move backwards the vacancy site. In the last case, the vacancy moves forwards.

Numerical simulations show that the occurrence of the three different cases depends highly on the relative phase of the incoming breather and the particles adjacent to the vacancy [22]. However, some conclusions can be extracted: 1) the incident breather always losses energy; 2) the breather can be reflected, trapped (with emission of energy) or transmitted by the vacancy, in analogy to the interaction moving breather-mass defect [24]; 3) the transmission of the breather (i.e. the breather passes through the vacancy) can only take place if the vacancy moves backwards, i.e. the particle to the left jumps one site in the direction of the breather. An explanation of this fact is that the particles to the right of the vacancy, in order to support a moving breather, need a strong interaction which cannot be provided by the interaction across a vacancy site, because the distance correspond to the soft part of the Morse potential. Fig. 9 illustrates these phenomena.

The moving breather–vacancy interaction is very sensitive to the velocity of the breather and the distance between the breather and the vacancy. Consequently, a systematic study of the state of the moving breather and the vacancy after the interaction cannot be performed. Therefore, we have performed a great number of simulations each one consisting in launching a single breather towards the vacancy site. In particular, we have chosen 1000 breathers following a Gaussian distribution of the perturbation parameter λ with mean value 0.13 and variance 0.03 for different values of the parameters b and C. Fig. 10(a) shows the probabilities that the vacancy remains at its original site, or that it jumps backwards or forwards, for $C = 0.5$ and $C = 0.4$. From this study, an important consequence can be extracted: concerning to the parameter b, there exist two different regions of values, separated by a critical value $b_0(C)$, such that for $b > b_0(C)$, the probability that the vacancy moves forwards is almost zero, whereas for $b < b_0(C)$, this probability is significant.

The non-existence of forwards vacancy migration can be explained through a bifurcation. These bifurcations are related to the disappearance of the entities we call *vacancy breathers*. They are defined as breathers centered at the site neighboring to the vacancy, e.g. the $n_v - 1$ or $n_v + 1$ sites. It can be observed in Fig. 10(b) that, for b below the bifurcation value, vacancy breathers do not exist.
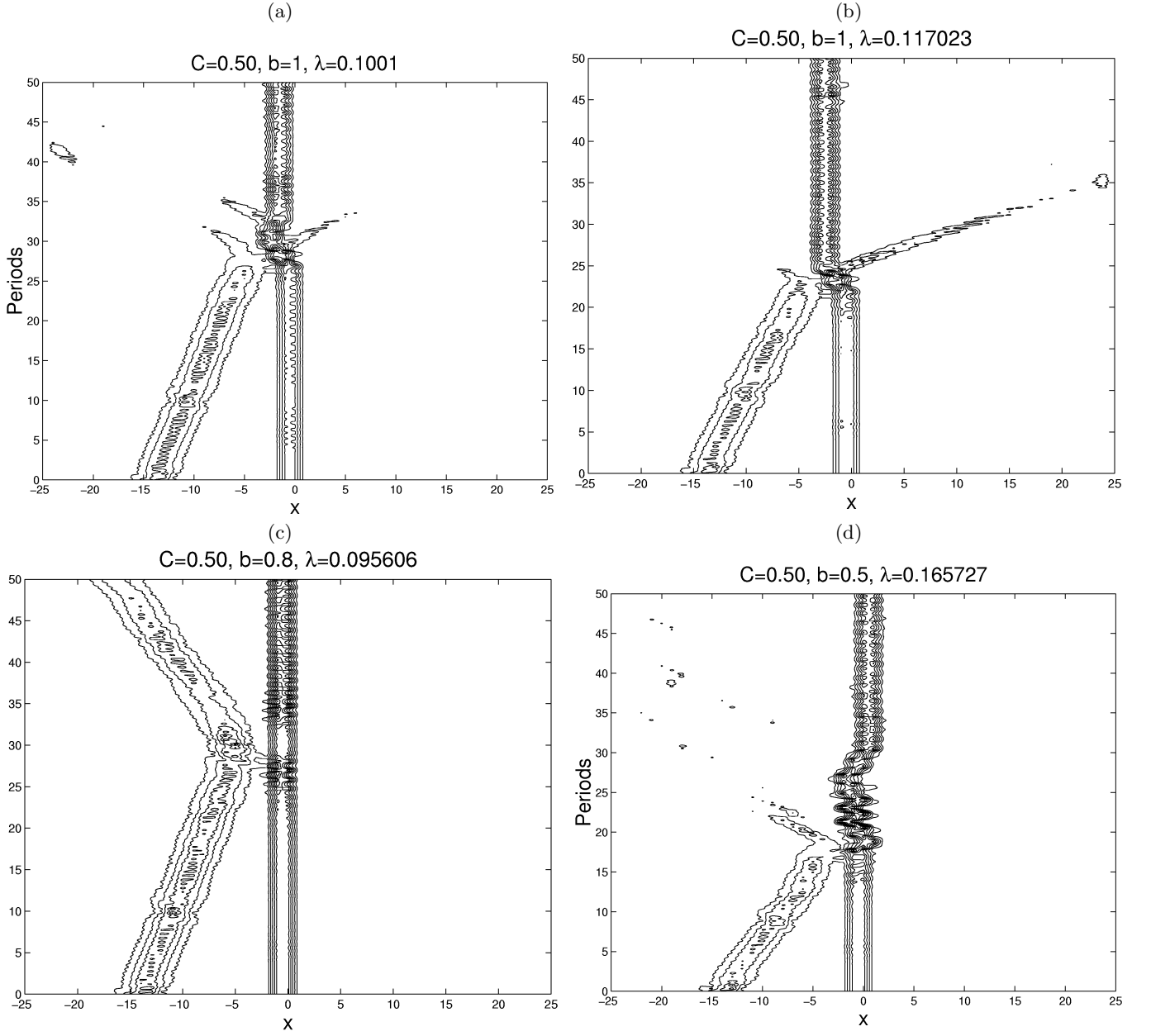
(a)

C=0.50, b=1, λ=0.1001

(b)

C=0.50, b=1, λ=0.117023

(c)

C=0.50, b=0.8, λ=0.095606

(d)

C=0.50, b=0.5, λ=0.165727

FIG. 9: Energy density plots of the interaction moving breather–vacancy. The vacancy is located at $n_{\rm v} = 0$. (a) the vacancy moves backwards; (b) the breather is transmitted by the vacancy; (c) the breather is reflected and the vacancy remains at rest; (d) the vacancy moves forwards.

VI. SMALL AND LARGE AMPLITUDE BREATHERS IN FERMI-PASTA-ULAM LATTICES

This section is dedicated to the study of breathers in Fermi-Pasta-Ulam (FPU) lattices, they can be considered as a subclass of the more generic Klein-Gordon lattices, in which the on-site potential term has been set to zero. An FPU lattice can be simply defined as a one-dimensional chain of particles subjected to nonlinear interactions between them. Therefore its Hamiltonian is given by

$$H = \sum_n \left[\frac{1}{2}\dot{x}_n^2 + W(x_n - x_{n-1}) \right], \tag{10}$$
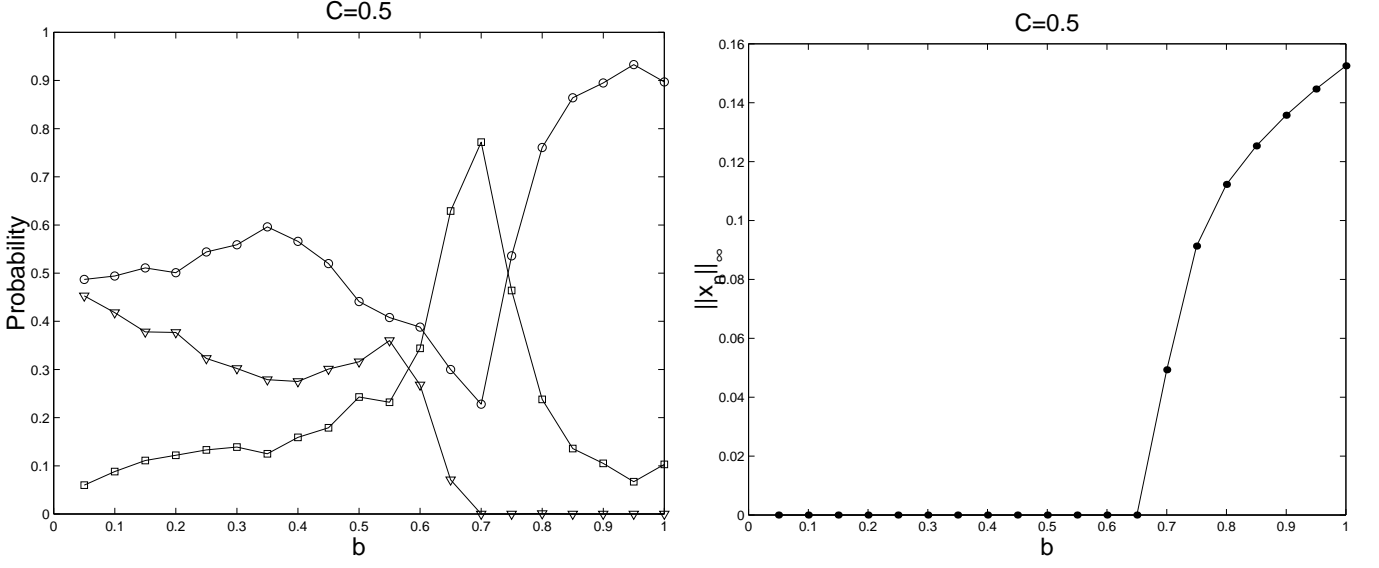
FIG. 10: (a) Probability that the vacancy remains at its site (squares), moves backwards (circles) or moves forwards (triangles), for a Gaussian distribution of λ as a function of the inverse potential width b. (b) Amplitude maxima of a vacancy breather versus b. The vacancy breather disappears at the bifurcation point. This is related to the vanishing of the forward movement probability.

where x_n describes the displacement of a particle from its equilibrium position, and $W(x)$ is a nonlinear interaction potential satisfying $W(0) = W'(0) = 0$, $W''(0) > 0$. A characteristic of this system is that it does not possess the so called "uncoupled limit", for which there exist trivial breathers. Although some early results on DBs were obtained in FPU chains in the late eighties by Sievers and Takeno [59], a complete and rigorous proof of their existence in these type of lattices was provided only some years ago. In 2001, using a variational method, Aubry *et al.* [12] proved the existence of breathers with frequency above the phonon spectrum if the non linear interaction potential, W, is a strictly convex polynomial of degree 4. In the same year and based on a center manifold technique, James [40] proved the existence (respectively, nonexistence) of small amplitude breathers (SAB) with frequency slightly above the phonon band if W satisfies (respectively, violates) the following local hardening condition:

$$B = \frac{1}{2}W^{(4)}(0) - (W^{(3)}(0))^2 > 0. \tag{11}$$

In spite of the implicit character of both proofs, the center manifold method provides additional information on the breathers amplitudes. In fact the method shows that for the interaction force $y_n = W'(u_n)$, all small amplitude time-periodic solutions with frequency ω_b of the FPU system (including breathers) have the form

$$y_n(t) = b_n \cos(\omega_b t) + \text{h.o.t}, \tag{12}$$

being the amplitudes b_n determined by the two-dimensional map

$$b_{n+1} + 2b_n + b_{n-1} = -\mu b_n + B b_n^3 + \text{h.o.t}, \tag{13}$$

provided ω_b lies near the upper edge, ω_π, of the phonon band, i.e. provided $\mu = \omega_b^2 - \omega_\pi^2 \ll 1$. For $B > 0$ fixed and $\mu > 0$ small enough, DBs correspond to homoclinic solutions to 0 of the recurrence relation (13) satisfying $\lim_{n \to \pm\infty} b_n = 0$. In Refs [40] and [41] an existence proof is given for two homoclinic solutions to 0, denoted as $\pm b_n^1$, $\pm b_n^2$, having different symmetries $b_{-n-1}^1 = -b_n^1$ (bond-centered mode) and $b_{-n}^2 = b_n^2$ (site-centered mode).

Since $0 < \mu \ll 1$ Eq. (13) can be approximated at leading order by an integrable differential equation [60] and it is easy to find the following approximations to the exact solutions y_n^1 and y_n^2:

$$y_n^1(t) \simeq (-1)^n \sqrt{\frac{2\mu}{B}} \frac{\cos \omega_b t}{\cosh((|n+1/2|-1/2)\sqrt{\mu})}, \tag{14}$$

$$y_n^2(t) \simeq (-1)^n \sqrt{\frac{2\mu}{B}} \frac{\cos \omega_b t}{\cosh(n\sqrt{\mu})} \quad . \tag{15}$$
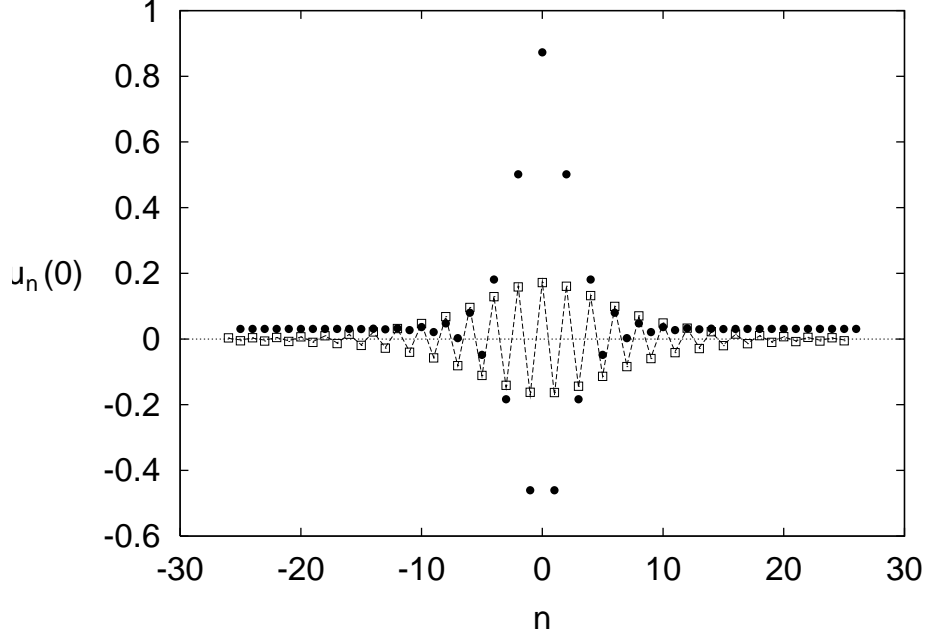
FIG. 11: Comparison between a small amplitude breather (squares) for $B > 0$ and a large amplitude breather (full circles) for $B < 0$ with the same frequency $w_b = 2.01$. This last breather is superposed to an uniformly static state given by $\lim_{n \to \pm\infty} u_n \approx 0.03$. The dashed line represents the centre manifold approximation (15) for small amplitude breathers. Parameters: SAB: $K_3 = -0.3$, $K_4 = 1$ ($B = 2.64$); LAB: $K_3 = -1$, $K_4 = 1$ ($B = -1$).

These expressions show that the maximum amplitude of SAB is

$$A \approx \sqrt{\frac{2\mu}{B}} \tag{16}$$

while their width is $O(\mu^{-1/2})$ and diverges as $w_b \to \omega_\pi^+$.

It is important to check the range of validity of the center manifold approximations (14), (15). A detailed numerical study of DBs in an FPU chain has been done [60] with the anharmonic potential

$$W(u) = \frac{u^2}{2} + \frac{K_3}{3}u^3 + \frac{K_4}{4}u^4 \tag{17}$$

and fixing $K_4 = 1$. With this choice $B = 3 - 4K_3^2$, and thus the parameter B is positive if $|K_3| < K_3^* = \sqrt{3}/2 \simeq 0.86$. In the case $K_3 = 0$ the potential is even with $B = 3 > 0$. For numerical convenience it is better to use as dynamical variables the difference displacements $u_n = x_n - x_{n-1}$. With these variables the equations of motions become

$$\ddot{u}_n + 2W'(u_n) - [W'(u_{n+1}) + W'(u_{n-1})] = 0 , \quad n \in \mathbb{Z} . \tag{18}$$

Note that u_n is one-to-one related to the forces y_n at small amplitudes, because W' is locally invertible since $W''(0) \neq 0$. Indeed, expressions (14), (15) also approximates u_n for small μ since $u_n = y_n + O(y_n^2)$. Moreover ussing periodic boundary conditions $u_{n+2p}(t) = u_n(t)$ the maximum frequency of the linear phonons, ω_π, is exactly 2 as in the infinite lattice.

As can be appreciated in Fig. 11, there exist an excellent agreement between the approximation (15) (dashed line) and an exact site-centered mode obtained numerically (squares) for $\omega_b = 2.01$ ($\mu \approx 0.04$) and $K_3 = -0.3$. Continuing this SAB as ω_b goes away from the phonon band, according to (16), the maximum amplitude of the relative displacements is approximately a linear function of $\mu^{1/2}$ up to $\mu \approx 2$, relatively far from the parameter region in which the center manifold approximation is valid in principle. In fact, the results show that, surprisingly, expressions (14) and (15) fit very well the profile of the relative displacements u_n even for breathers with moderate amplitudes.

The linear stability of the SAB can be studied through a Floquet analysis [10]. In the symmetric potential case the result is well known [15]: the Page mode (site-centred mode in the u_n variables) is stable while the Sievers-Takeno

mode (bond-centred mode in the u_n variables) has a harmonic instability (a pair of real eigenvalues σ, σ^{-1} close to 1) that increases with the breather frequency. When a cubic term in the potential W is introduced ($K_3 \neq 0$), the situation is more complex. Non-even potentials induce oscillatory instabilities in both modes, which increase with $|K_3|$. Although most of the oscillatory instabilities are size dependent effects, some of them survive in the limit of an infinite lattice. Thus in the non-even potential case, both modes turn out to be unstable [34]. The recurrence relation (13) assures that SAB with frequencies slightly above the phonon band do not exist for $B < 0$ ($\sqrt{3K_4}/2 < |K_3|$). However, in this parameter region numerical simulations show that there exist breathers whose amplitudes do not tend to zero as $w_b \to 2^+$ [60]. As a consequence the energies of this family of breathesrs lay always above a certain positive lower bound. The existence of such an energy threshold is a rarely observed phenomenon in one-dimensional lattices. [43]

The breathers obtained for $B < 0$ have the same symmetries (site-centred and bond-centred modes) and the same stability properties as SAB with non-even potentials, i.e. both modes show oscillatory instabilities and also a harmonic instability in the case of the Sievers-Takeno mode.

Another interesting problem is the study of breathers superposed to uniformly stressed static states of the FPU chain given by $x_n = c\,n$, being c a nonzero constant [55]. Introducing the change of variables $x_n(t) = cn + \tilde{x}_n(t\,\sqrt{W''(c)})$, the previous analytical and numerical analysis can be completely applied to the renormalized displacements $\tilde{x}_n$ [60]. As a consequence, it is easy to prove that the FPU model has a family of exact breather solutions satisfying $\lim_{n \to \pm\infty} u_n = c$, which can be approximated by

$$u_n(t) \simeq c + (-1)^n \sqrt{\frac{2\mu}{B(c)}} \frac{\cos(\omega_b t)}{\cosh(n\sqrt{\mu/W''(c)})}, \tag{19}$$

where $\mu = \omega_b^2 - 4\,W''(c) \ll 1$, and $B(c) = \frac{1}{2}W''(c)\,W^{(4)}(c) - (W^{(3)}(c))^2 > 0$. An example of a breather with a uniform stress is shown in Fig. 11 with full circles. Note that the lower frequency of these breather solutions lies inside the phonon band if $W''(c) < 1$, and above it for $W''(c) > 1$.

VII.   DARK BREATHERS IN KLEIN–GORDON LATTICES

The study of breathers in chains of nonlineraly interacting particles has a natural extension in the study of other localized entities called "dark breathers". The term dark breather refers to a state of the chain where most of the oscillators are excited except one or a few units of them which have a very small amplitude. That is, in some sense it posses the opposite properties than a breather. This section summarizes some results about the conditions for the existence and stability properties of dark breathers in different Klein–Gordon lattices.

Consider one–dimensional Klein–Gordon lattices of oscillators with Hamiltonian

$$H = \sum_n (\frac{1}{2}\,\dot{u}_n^2 + V(u_n)) + \varepsilon\,W(u), \tag{20}$$

where u_n represents the coordinates of the oscillators referred to their equilibrium positions; $V(u_n)$ represents the on–site potential; u represents the set of variables $\{u_n\}$; and $\varepsilon W(u)$ represents the interacting potential. The parameter ε describes the intensity of the coupling, and $W(u)$ is given by

$$W(u) = \frac{1}{2} \sum_n (u_{n+1} - u_n)^2. \tag{21}$$

This interaction is attractive for $\epsilon > 0$, as a nonzero value of a variable tends to increase the values of the neighbouring variables with the same sign. The on–site potential is given by

$$V(u_n) = \frac{1}{2}\,\omega_0^2\,u_n^2 + \phi(u_n), \tag{22}$$

with $\phi(u_n)$ being the anharmonic part of the potential. The variables can be scaled so that all the particles in the lattice have mass unity and the linear frequency $\omega_0 = 1$.

The existence theorem by Mackay and Aubry [46] establishes that dark breather solutions are possible, at least up to a certain value of the coupling parameter ε_c. Dark breathers can be calculated numerically. The method to calculate this type of solutions is similar to the used for obtaining breathers [3]. Fig. refFig12, shows two different examples of dark breather profiles for a chain with a cubic soft on–site potential, with attractive interaction (left panel), and with repulsive interaction (right panel).
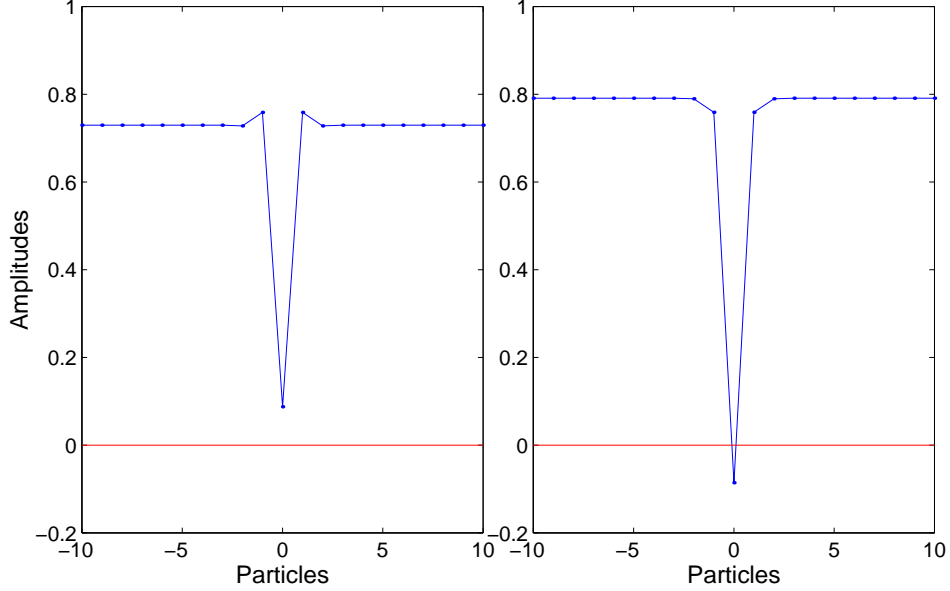
FIG. 12: Dark breathers profile for a cubic potential with attractive interaction (left) and with repulsive interaction(right), with $\varepsilon = 0.023$.

The linear stability analysis of dark breather solutions can be performed numerically. For that porpose both the Floquet multipliers and the Aubry band theory can be considered [10, 50].

In the case of a soft on–site potential of the type $\phi(u_n) = -\frac{1}{3}u_n^3$, and attractive interaction between particles, dark breather solutions are not stable. Fig. 13 shows the type of stability of a dark breather and a breather by the Floquet multipliers method. The breather (left) is stable for $\epsilon \leq 0.1$, whereas the dark breather (right) is unstable for all the ϵ values considered. This instability is due to harmonic bifurcations.

Considering chains with repulsive interactions, the linear stability analysis shows that dark breather solutions are stable up to a significant value of the parameter ϵ.

The type of stability behaviour described above appears also in other kind of soft on–site potentials as, for example, the Morse potential given by

$$V(u_n) = D\left(\exp(-bu_n) - 1\right)^2. \tag{23}$$

Dark breather solutions are stable if the coupling is repulsive for $\epsilon \leq 0.024$. For bigger values the solution becomes unstable due to oscillatory and subharmonic bifurcations [3]. Fig. 14 shows the evolution of the Floquet multipliers for $\epsilon = 0.024$ (left panel), where the dark breather solution is still stable, and for $\epsilon > 0.024$ (right panel), where oscillatory and subharmonic bifurcations appear.

Lattices with hard on–site potential present a different scenario. The dark breather solution is stable with attractive coupling potential, up to a certain value of ϵ, and is unstable if the coupling is repulsive. Oscillatory, subharmonic and harmonic bifurcations appear depending on the form of the on–site potential. For a hard on–site potential of the type $\phi(u_n) = \frac{1}{4}u_n^4$ and attractive coupling, the system is stable for $\epsilon \leq 0.022$. Figs. 15 and 14 represent, respectively, the band structure and the Floquet multipliers at $\epsilon = 0.041$. They show that the dark breather solution is unstable due to an harmonic and small oscillatory bifurcations. The instability mode, shown in Fig. 15 (right panel), is an asymmetric extended one. Simulations performed perturbing with it the dark breather give rise to a small oscillation with both sides of the chain out of phase, superimposed on the dark breather one, but the darkness is preserved. After that, there are oscillatory bifurcations due to the band mixing with the usual properties.

An analysis of larger systems shows that subharmonic and oscillatory bifurcations persist even though the system is infinite, while in the case of breathers there are two kinds of size–dependent bifurcation [49].
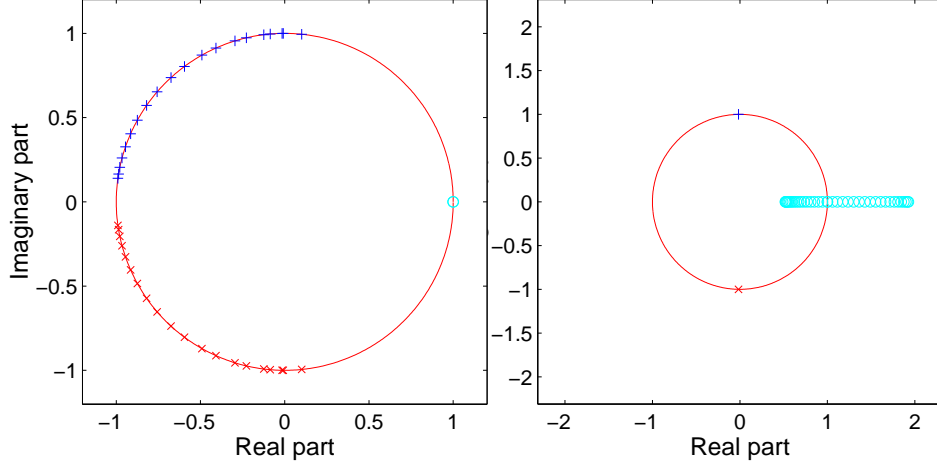
FIG. 13: Evolution of the Floquet multipliers with cubic on–site potential and attractive interaction for: (left) a breather with $\varepsilon = 0.1$; (right) a dark breather with $\varepsilon = 0.004$. The breather frequency is in both cases $\omega_\mathrm{b} = 0.8$.
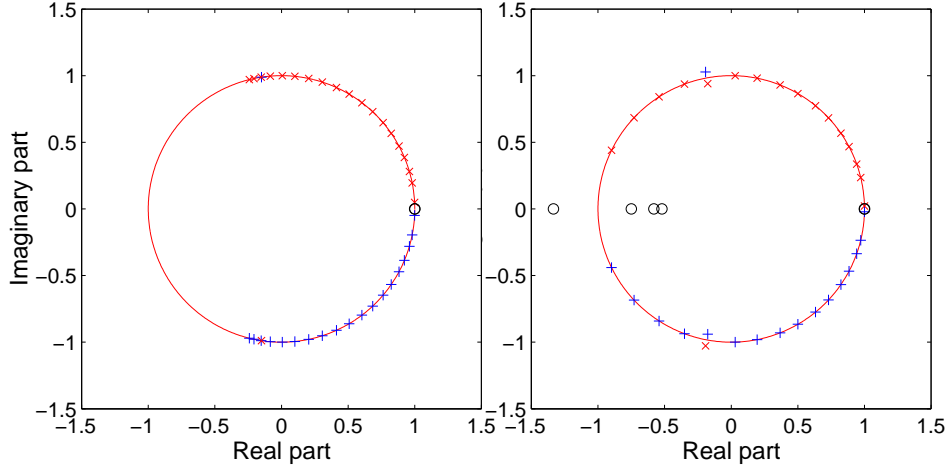

FIG. 14: Floquet eigenvalues for a Morse on–site potential and repulsive coupling. Left: $\varepsilon = 0.024$, the system is still stable. Right: $\varepsilon = 0.035$, the system becomes unstable due to oscillatory and subharmonic bifurcations.

VIII.   POLARONS IN BIOMOLECULES

The study of charge transport (CT) in biomolecules, and particularly in DNA, is of utmost importance. Electronic transport plays a very important role in many biological processes, such as DNA repair after damage by radiation or chemical agents, photosynthesis, nevous conduction, etc. Also, because the quasi–one–dimensional structure of DNA and other biomolecules could be used to design electronic devices based on biomaterials (for a detailed bibliographical information, see i.e. [38]).

When an electron moves along the double strand of DNA it is accompanied by a local deformation of the molecule, forming a polaron or an electron–vibron breather. The polaronic character of the CT along DNA has been studied by means of different models, some of then based on the Peyrard–Bishop DNA model [53], in which the only variables are the distances between bases within each base pair. have permitted to show that the polaronic charge transport
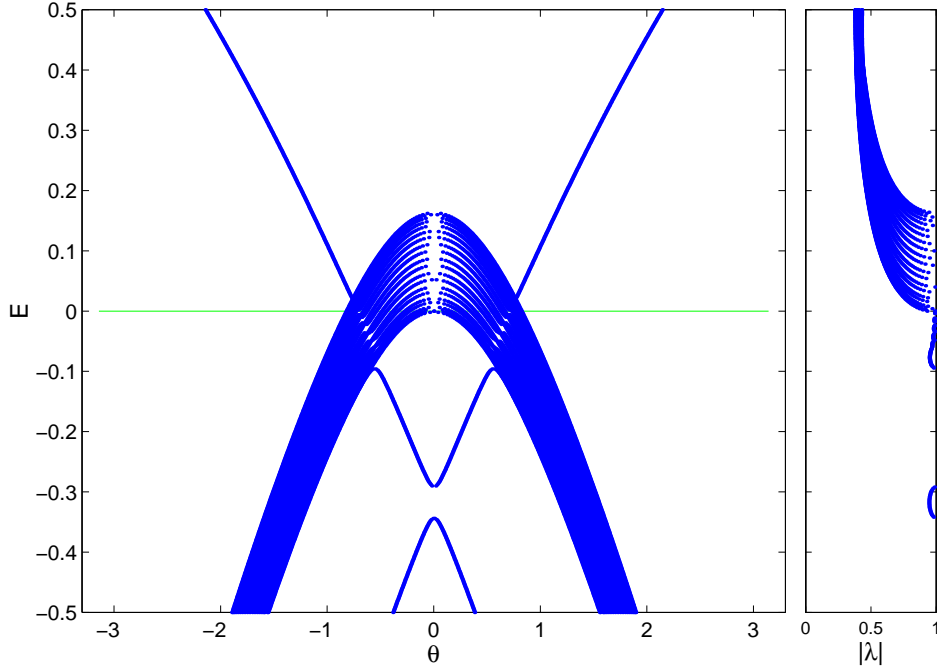
FIG. 15: Band structure for a quartic hard on–site potential with attractive interaction at $\varepsilon = 0.041$ and $\omega_b = 1.2$.
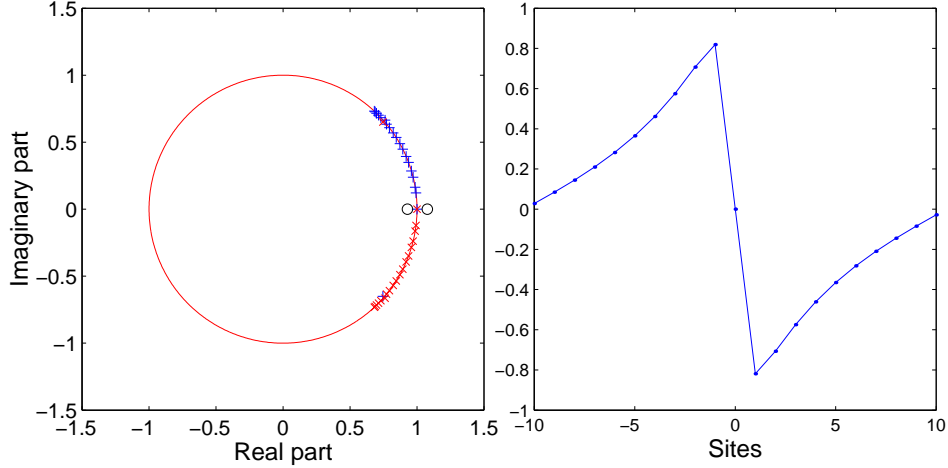

FIG. 16: Left: Floquet multipliers with a quartic hard on–site potential and attractive interaction at $\varepsilon = 0.041$ and $\omega_b = 1.2$. A harmonic and a small oscillatory instabilities appear. Right: the velocities components (the position ones are zero) of the eigenvalue corresponding to the harmonic instability.

along DNA can be mediated by the coupling of the charge carrying unit with the hydrogen–bond deformations,

   In particular, it has been shown in some simple, but powerful models based on the proposed by Peyrard–Bishop [53], that the polaronic CRT along DNA can be mediated by coupling of the charge carrying unit with the hydrogen–bond deformations, and that this transport survives to a small amount of parametric and structural disorder [37], or by means of the coupling of this charge unit with the twist deformation of neighbor base pairs [52]. In this last case, the moving polaron is slower than in the previous one, but it is more robust under the introduction of parametric disorder. These differents regimes apperars for different values of a parameter α, the couples the transference integral with the deformations of the hydrogen bonds, a parameter which at present there is not any realible experimental data.

   Consider a three-dimensional semi–classical tight–binding model for synthetically produced DNA polymers built up
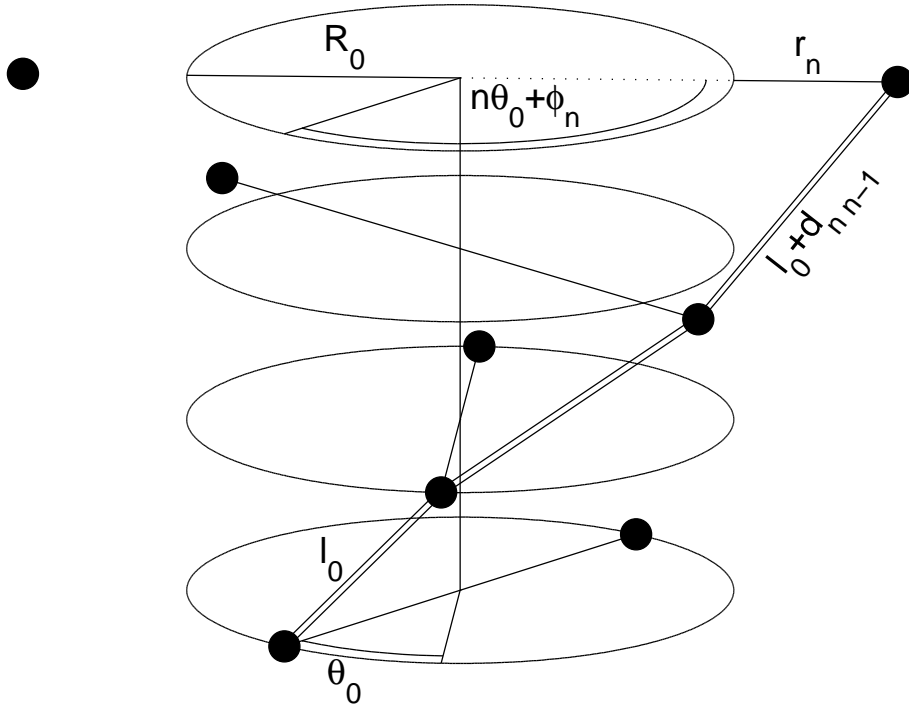
FIG. 17: Sketch of the structure of the DNA model. The bases are represented by bullets.

from single type of base pairs, i.e. either poly(dG)-poly(dC) or poly(dA)-poly(dT) DNA polymers [54]. Utilizing a nonlinear approach based on the concept of breather and polaron solutions it is possible to explore if the conductivity depends on the type of the DNA polymer. If they have quantitatively distinct transpor properties or not might be of interest for the design of synthetic molecular wires. Moreover, it has been possible to ameliorate preceding studies of electronic transfer in DNA [37], [36] in the sense that, instead of adjusting the coupling parameters, plausible estimates for them, derived with the help of quantum-chemical methods, has been used.

The model for CT in DNA is based on the finding that the charge migration process is dominantly influenced by the transverse vibrations of the bases relative to each other in radial direction within a base pair plane. The impact of other vibrational degrees of freedom are expected to be negligible with respect to charge transport in DNA. Then, the motion can be viewed as confined to the base pair planes [61]. The Hamiltonian for CT in along a strand in DNA has two parts $H = H_{el} + H_{vib}$, with H_{el} describing the CT over the base pairs and H_{vib} the dynamics of radial vibrations of the base pairs or the vibronic part. A sketch of the structure of the DNA model is shown in Fig. 17.

Supposing that vibrational dynamics can be described classically, it is easy to formulate the dynamical equations of the system (a detailed description of procedure can be found in [52]).It is possible to use some typical parameter values for DNA molecules and compute plausible values for the electron–coupling strengths as a result of quantum–chemical computational procedure [38].

The nonlinear interplay between the electronic and the vibrational degrees of freedom, makes possible the formation of polaronic electron–vibration compounds. Also, there exist some stationary solutions that can be calculated with the help of the nonlinear map approach explained in detail in [42]. In general, the polarons are of fairly large extension (width). Regardless of the DNA polymer type, the electronic wave function is localized at a lattice site and the envelope of the amplitudes decays monotonically and exponentially as distance grows from this central site (base pair). However, the electronic wave function of the poly(dG)-poly(dC) DNA polymer is stronger localized than the one of its poly(dA)-poly(dT) counterpart. As polarons solutions are fairly large extended (the half-width involves $\lesssim 100$ lattice sites) it is plausible to think that the can be mobile. This polaron motion can be activated using the discrete gradient method to obtain suitable initial perturbations of the momentum coordinates which initiate coherent motion of the polaron compound. The electronic occupation probability is defined as $\bar{n}(t) = \sum_n n \, |c_n(t)|^2$, where the index n denotes the site of the $n-$th base on a strand and c_n determines the probability to find the electron (charge) residing at this site.

Results relative to the time evolution of the first momentum of the electronic occupation probability are shown in Fig. 18. Conductivity in synthetically produced DNA molecules depends on the type of the single base pair

of which the polymer is built of. While a polaron-like mechanism, relying on the nonlinear coupling between the electron amplitude and radial vibrations of the base pairs, is responsible for long-range and stable electronic transfer in (dG)-(dC) DNA polymers, the conductivity is comparatively weaker in the case of (dA)-(dT) DNA polymers. Especially when it comes to designing synthetic molecular wires these findings might be of interest. In fact, recent experiments suggest that electronic transfer through DNA molecules proceeds by polaron hopping [44]. Furthermore, these results comply with the findings of experiments which show also that poly(dG)-poly(dC) DNA polymers forms a better conductor than their poly(dA)-poly(dT) counterparts.
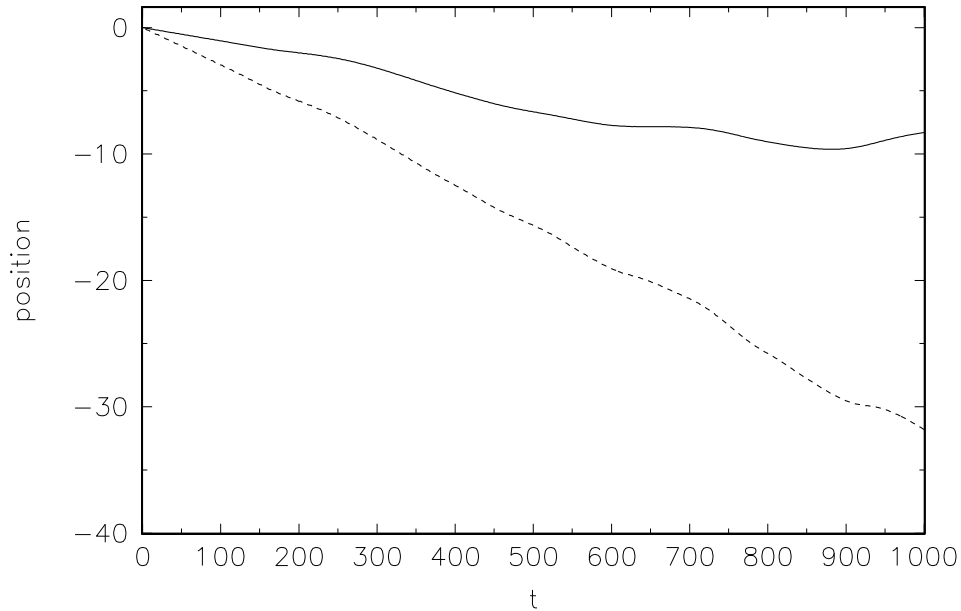

FIG. 18: Time evolution of the first momentum of the electronic occupation probability. Full (dashed) line: poly(dA)-poly(dT) (poly(dG)-poly(dC)) DNA polymer.

IX. QUANTUM BREATHERS

At present, the phenomenon of localization of energy due to nonlinearity in discrete classical lattices is relatively well understood, but the understanding of the quantum equivalence of discrete breathers is very limited. There exist some theoretical results [28, 58] and some experimental observations of these states in different quantum systems, as mixtures of 4–methyl–pyridine [33], in Cu benzoate [9], and in doped alkalihalides [56]. Also, the study of discrete breathers in quantum lattices supporting a small number of quanta is not only interesting theoretically, this knowledge may be relevant to studies of quantum dots and quantum computing [45], and for studies of Bose–Einstein condensates trapped in optical traps [2].

This section focus the attention in one–dimensional lattices with a small number of quanta described by the the quantum version of the discrete nonlinear Schrödinger equation (QDNLS), also known as the Hubbard model. This is a particularly simple model for a lattice of coupled anharmonic oscillators, which has been used to describe the dynamics of a great variety of systems [57]. We present the results corresponding to a periodic lattice with f sites containing bosons [30]. Many of these results can be extended to a great variety of systems, for example, similar results have been obtained with a periodic lattice containing fermions, described by an attractive fermionic Hubbard model (FH) with two kinds of particles with opposite spins. This is a model of interest in connection with the theory of high-T_c superconductivity, and it can be used to describe bound states of electron and holes in some nanostructures as nanorings (excitons) [29].

The QDNLS Hamiltonian of the quantum system is

$$\hat{H} = -\sum_{j=1}^{f} \frac{1}{2}\gamma_j b_j^\dagger b_j^\dagger b_j b_j + \epsilon_j b_j^\dagger (b_{j-1} + b_{j+1}), \tag{24}$$

where $b_j^\dagger$ and b_j are standard bosonic operators, γ_j/ϵ_j is the ratio of anharmonicity to nearest neighbor hopping energy, and periodic boundary conditions are imposed. As first step, only short range interactions are considered given by the hopping coefficients ϵ_j.

This Hamiltonian conmutes with the number operator $N = \sum_{j=1}^f b_j^\dagger b_j$, and can be block-diagonalised easily when the number of bosons is small enough. Numerically exact solutions can be found restricting the study to small lattices with a small number of quanta. The simplest nontrivial case is for $N = 2$, where bound states corresponds to bound two-vibron states, as has been observed experimentally in several systems [39]. These results have been extended to more complicated situations, noting that many of them are valid for larger values of N.

A. Quantum breathers in a translational invariant lattice

In a homogeneous quantum lattice the parameters γ_j and ϵ_j are independent of j, i.e. $\gamma_j = \gamma$ and $\epsilon_j = \epsilon$. With periodic boundary conditions, it is possible to block–diagonalize the Hamiltonian operator using eigenfunctions of the translation operator $\hat{T}$, defined as $\hat{T} b_j^\dagger = b_{j+1}^\dagger \hat{T}$. In each block, the eigenfunctions have a fixed value of the momentum k, with $\tau = \exp(ik)$ being an eigenvalue of the translation operator [57]. In this way, it is possible to calculate the dispersion relation $E(k)$ with a minimal computational effort.

In general, as shown in 19, if parameter γ is high enough, there exists an isolated ground state eigenvalue for each k which corresponds to a quantum breather. In this state, there is a high probability of finding the quanta on the same site, but due to the translational invariance of the system, there exists an equal probability of finding these quanta at any site of the system. In these cases, some analytical expressions can be obtained in some asymptotic limits [57].
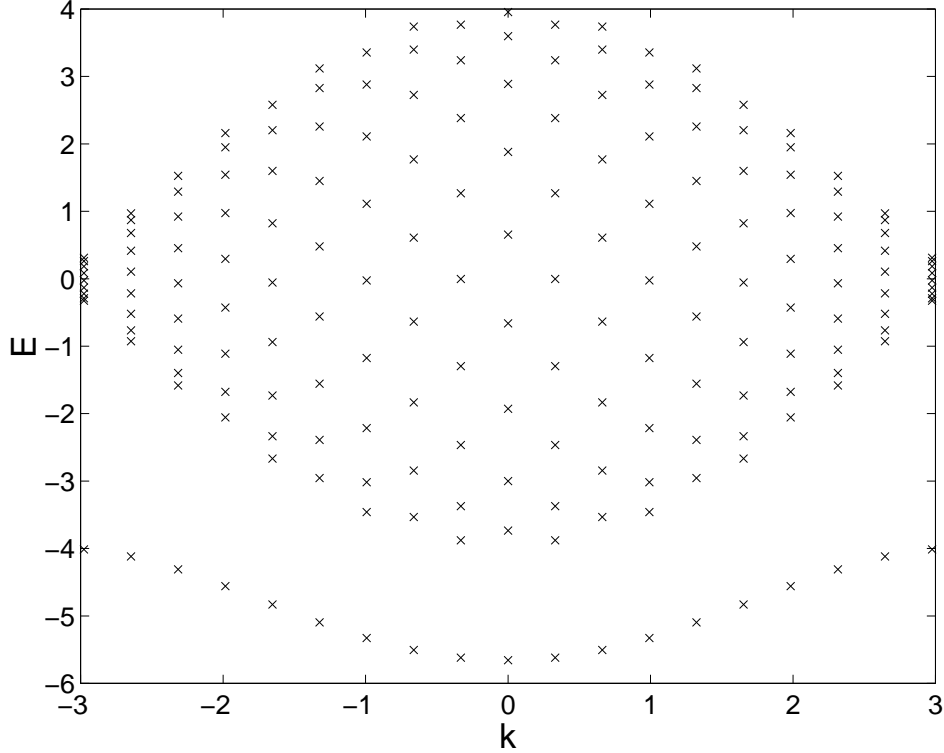

FIG. 19: Eigenvalues $E(k)$. $N = 2$, $f = 19$ and $\gamma = 4$.

For example, using the number–state–basis $|\psi_n> = [n_1^a, n_2^a, ..., n_f^a]$, where n_i^a represents the number of quanta at site i, in the case $N = 2$ and $k = 0$ the (unnormalized) ground state is given by

$$|\Psi\rangle = [20\dots0] + [020\dots0] + \cdots + [0\dots02] + O(\gamma^{-1}).$$

The coefficients a_i of the first f terms are equal to unity and the rest are $O(\gamma^{-1})$.

B.   Trapping in lattices with broken translational symmetry

When the translational invariance of a lattice is broken, the Hamiltonian operator does not commute with the translation operator and breathers can be localized around a particular point of the lattice. Perhaps the simplest way to do it is to consider non–flux boundary conditions, in order to simulate a finete–size chain. In this case, the ground state becomes localized around the middle of the chain but, when f is high enough, this effect vanishes.

The existence of local inhomogeneities or impurities can also break the translational symmetry of the system, and this can be modeled by making some coefficients dependent on the site. This can occurs in system with twisted or bent geometries, as in models of globular proteins [31] or photonic crystals In these cases, the geometry effects can be considered introducing a long–range hopping term in the Hamiltonian operator.

The breaking of translational symmetry of the system localizes the breather state around a particular site of the chain, as shown in Fig. 20. Note that the localization phenomena due to random variation of lattice parameters have been studied in harmonic models since the work of Anderson [4] but, in all cases, and due to anharmonic effects, there exist new localization effects, and, when it is present, the anharmonicity enhances the Anderson–like effect.
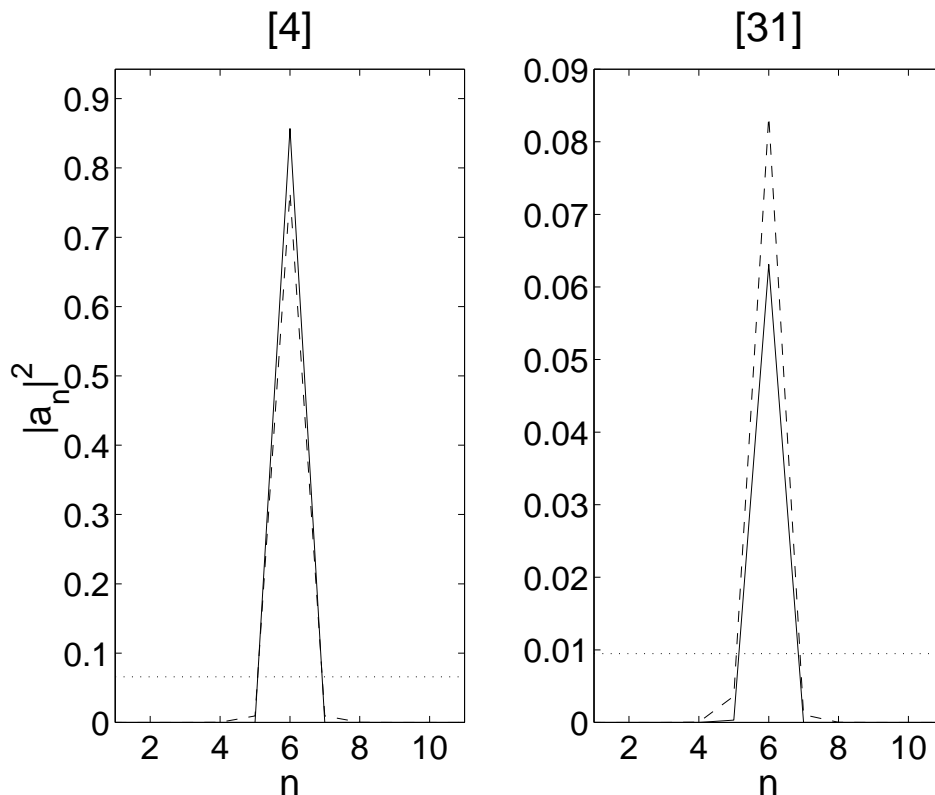

FIG. 20: Square wave function amplitudes corresponding to localized components of the ground state. $f = 11$, $N = 4$ and $\gamma = 2$. Point impurity at the site $\ell = 6$. ($\cdots$) homogeneous chain case, $\gamma_{\mathrm{im}} = 2$, (- - -) $\gamma_{\mathrm{im}} = 2.1$, (——) $\gamma_{\mathrm{im}} = 2.5$.

X.   THERMAL EVOLUTION OF ENZYME-CREATED OSCILLATING BUBBLES IN DNA

This last section reviews some fundamental researches on the creation and subsequent evolution of breathers in DNA chains. For a double–stranded DNA molecule to replicate, the two strands of the double helix must be separated from each other, at least locally, with the breaking up of the hydrogen bonds. For long double–stranded DNA molecules, the rate of spontaneous strand separation is very low under physiological condition. Specific enzymes belonging to the large family of nucleic acid helicases (see [61]) (there are more than sixty different types), utilize the energy of ATP hydrolysis to power strand separation. The opening of a selected region of the twisted (Watson-Crick) DNA double helix, begins with a partial unwinding at an area called the replication fork and is observed as a bubble. Helicases are ubiquitous and versatile enzymes that, in conjunction with other components of the macromolecular machines,

carry out important biological processes such as DNA replication; DNA recombination; nucleotide excision repair (i.e. UV damage); RNA editing and splicing; the transfer of a single-stranded nucleic acid to other nucleic acid or a protein or its release into solution [62] and formation of T-loop telomeres [63]. Nucleic acid helicases have several structural varieties (monomeric, dimeric, trimeric, tetrameric and closed hexameric), but all of them use the hydrolysis of nucleoside triphosphate (NTP) to nucleoside diphosphate (NDP) as the preferred source of energy. Helicases have also a huge interest from a point of view of clinical disease. Actually, there are known up to five human monogenic hereditary disorders in which the mutated protein responsible for the disease carries an aberrant helicase activity: cockayne 's syndrome, xeroderma pigmentosum, trichothiodystrophy, Bloom 's syndrome, and Werner 's syndrome. The study of the formation of DNA openings has been initiated recently utilizing models based on nonlinear lattice dynamics [1, 32].

With a view to vibrational excitations in DNA, the Peyrard–Bishop (PB) model [53] and its successors [14, 26] have been successfully applied to describe moving localized excitations (moving breathers), which reproduce typical features of the DNA opening dynamics such as the magnitude of the amplitudes and the time scale of the "oscillating bubble" preceding full strand separation.

The bubble formation process is initiated by structural deformations of selected regions of the parental DNA duplex that serves as a template for the replication. The process begins when the replication apparatus identifies the starting point and then gets combined to it. The replication apparatus is and assembled complex that forms the replication fork and opens it directionally. During this process the helical DNA is unwound and replicated. One of the components of that complex a type of helicase, which is unable to recognize the origin of the replication *per se*, and which requires the participation of specific proteins to lead it to the initiation site [27].

It is assumed that this enzyme operates in the way, that a local unwinding in combination with (rather small) stretchings of the H-bonds in this region occurs. A working model should demonstrate that there are indeed initial deformations that give rise to localized vibrations, constrained to a region of DNA, matching the properties of oscillating bubbles observed experimentally. These oscillating bubbles with their temporarily extended but yet unbroken H-bonds serve as the precursors to the replication bubble. Furthermore, it is important to know whether the stable radial and torsional breathers persist under imposed thermal perturbations.

The research has been done using a nonlinear oscillator network model for the DNA double helix that is explained in detail in [1, 14, 18]. The equilibrium position of each base within the duplex configuration is described in a Cartesian coordinate system by $x_{n,i}^{(0)}$, $y_{n,i}^{(0)}$ and $z_{n,i}^{(0)}$. The index pair (n, i) labels the n-th base on the $i-$th strand with $i = 1, 2$ and $1 \leqq n \leqq N$, where N is the number of base pairs considered. Displacements of the bases from their equilibrium positions are denoted by $x_{n,i}$, $y_{n,i}$ and $z_{n,i}$. The potential energy taking into account the interactions between the bases consists of four parts. The potential energy of the hydrogen bond within a base pair is modeled typically by a Morse potential

$$V_h^n = D_n \left[\exp\left(-\frac{\alpha}{2} d_n \right) - 1 \right]^2 , \tag{25}$$

where the variables d_n describe dynamical deviations of the hydrogen bonds from their equilibrium lengths d_0. The site-dependent depth of the Morse potential, D_n, depends on the number of involved hydrogen bonds for the two different pairings in DNA, namely the G-C and the A-T pairs. The former pair includes three hydrogen bonds while the latter includes only two. α^{-1} is a measure of the potential–well width.

The energies of the rather strong and rigid covalent bonds between the nucleotides n and $n-1$ on the $i-th$ strand are modeled by harmonic potential terms

$$V_c^{n,i} = \frac{K}{2} l_{n,i}^2 , \tag{26}$$

and $l_{n,i}$ describes the deviations from the equilibrium distance between two adjacent bases on the same strand. K is the elasticity coefficient.

Effects of stacking, which impede that, due to the backbone rigidity, one base slides over another [61] are incorporated in the following potential terms

$$V_s^{n,i} = \frac{S}{2} (d_{n,i} - d_{n-1,i})^2 . \tag{27}$$

The supposedly small deformations in longitudinal direction can be modeled by harmonic elasticity potential terms given by

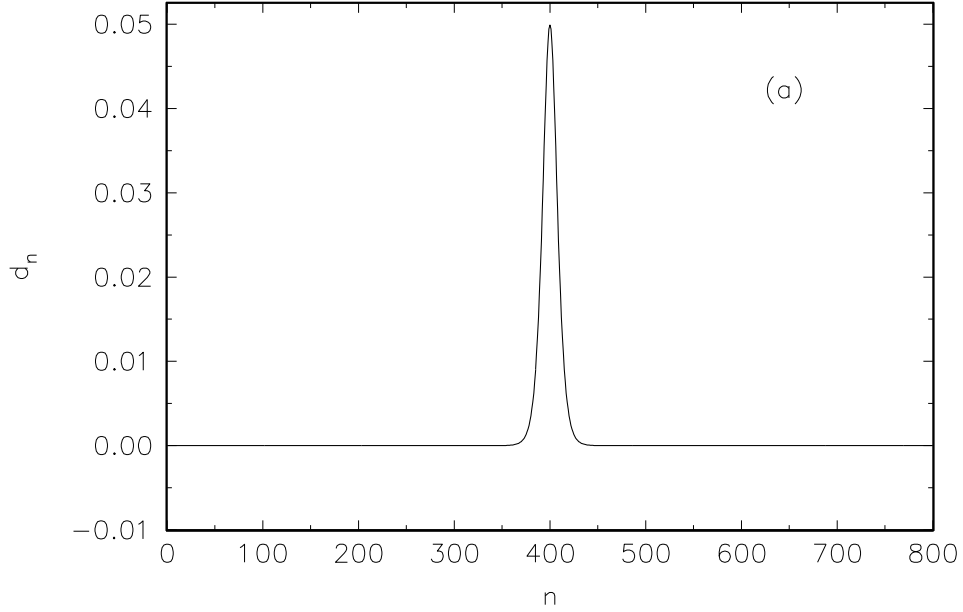$$V_l^{n,i} = \frac{C}{2} (z_{n,i} - z_{n-1,i})^2 . \tag{28}$$

FIG. 21: The initial radial distortions of the double helix. The inter-base distance $d_n(0)$ in Å.

The kinetic energy of a nucleotide is determined by

$$E_{kin}^{n,i} = \frac{1}{2m} \left[\left(p_{n,i}^{(x)} \right)^2 + \left(p_{n,i}^{(y)} \right)^2 + \left(p_{n,i}^{(z)} \right)^2 \right], \tag{29}$$

where m is the mass and $p_{n,i}^{(x,y,z)}$ denotes the (x,y,z)−component of the momentum.

The model Hamiltonian reads then as

$$H = \sum_{i=1,2} \sum_{n=1}^{N} E^{n,i}, \tag{30}$$

with

$$E_{n,i} = E_{kin}^{n,i} + V_h^n + V_c^n + V_s^{n,i} + V_l^{n,i}, \tag{31}$$

and the summation in (30) is performed over all nucleotides and the two strands.

Consider the initiation of the oscillating bubbles in DNA. The starting point is a DNA molecule for which a certain segment experiences initially angular and radial deformations due to the action of some helicase to which a region of the DNA is bound. In order to simulate the deforming action of enzymes, assume that initially a number of consecutive sites in the center of the DNA lattice (hereafter referred to as the *central region*) are exerted to forces acting in angular and radial direction such that in this region the molecule experiences twist reduction together with radial stretchings. These structural deformations can be extended over a region encompassing up to thirty base pairs and as can be demonstrated give rise to the formation of H-bridge breather solutions (extending over $15 - 20$ base pairs) reproducing the "oscillating bubbles" observed for the DNA-opening process [13]. In Figs. 21 and 22 the localized initial distortions are shown. Both the angular and radial deformation patterns are bell-shaped, due to the fact that the enzymatic force is exerted locally, i.e. in the extreme case to a single base pair only for which the H-bond is deformed

The first one being of non-positive amplitudes is linked with reduced twist while the latter one with non-negative amplitudes is associated with radial stretchings. The radial and angular deformation patterns are centered at the central lattice site (base pair) at which the H-bond stretching and twist angle reduction is at maximum. At either side of the central site the amplitudes approach progressively zero. The deformation energy amounts to $0.0362\,\mathrm{eV}$. The associated set of coupled equations has been integrated with the help of a fourth-order Runge-Kutta method. For the simulation the DNA lattice consists of 799 sites and open boundary conditions are imposed. The same initial conditions are used both at zero and nonzero temperatures.

The study of the temperature dependence of these oscillating bubbles has been done by means of bringing in contact the nonlinear oscillator network with a heat bath using the Nos-Hoover-method. It is demonstrated that the radial and
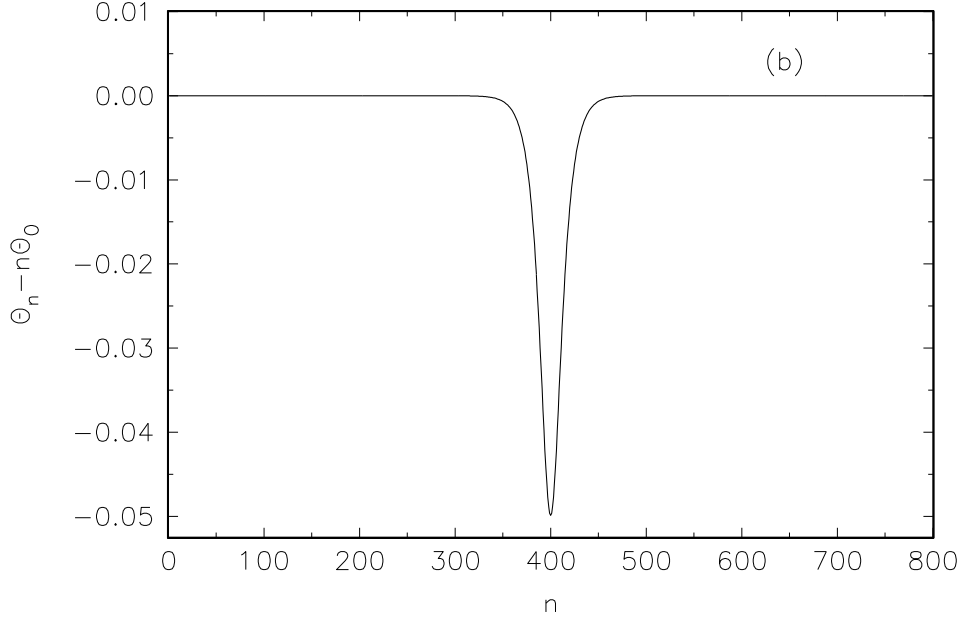
FIG. 22: The initial angular distortions of the double helix.

torsional breathers sustain the impact of thermal perturbations, even at temperatures as high as room temperature. For T¿0 the breathers start to travel coherently towards an end of te DNA duplex, representing realistically the oscillating bubbles found in NAs i.e. they oscillate with periods in the range 0.3 -0.8 ps, are on the average extended over 10 -20 base pairs and possess maximal amplitudes of the order of 0.6 A.

Quantitatively, the results regarding the temperature dependence of the breather evolution are suitably summarized by the time-evolution of the first momentum of the energy distribution defined as

$$\bar{n}(t) = \sum_{i=1,2} \sum_{n=1}^{N} (n_c - n) E_{n,i}(t), \tag{32}$$

and the energy $E_{n,i}$ is defined in Eq. (31) and n_c is the site index corresponding to the center of the DNA lattice.

This quantity describes the temporal behavior of the position of the center of a breather. Thus it represents a measure for the mobility of the breathers. Generally, the higher the temperature the larger the amplitude of the radial breather becomes and the faster the radial (and torsional) breather travels along the DNA lattice. This behavior is illustrated in Fig. 23.

In summary, out of an initial non-equilibrium situation, for which the hydrogen bonds of an under-twisted segment of the DNA lattice have been stretched, breathers develop in the radial and angular displacement variables. For zero temperature the breathers remain standing in the initially excited region. However, for $T > 0$ the breathers start to travel coherently towards an end of the DNA duplex. The observed breathers represent realistically the oscillating bubbles found prior to complete unzipping of DNA, i.e. they oscillate with periods in the range $0.3 - 0.8 \, ps$, are on the average extended over $10 - 20$ base pairs and possess maximal amplitudes of the order of $\lesssim 0.6 \, \text{Å}$. These results demonstrate that the action of some enzyme, mimicked by localized radial and torsional distortions of the DNA equilibrium configuration, initiates in fact the production of oscillating bubbles in DNA. Moreover, these "oscillating bubbles" sustain the impact of thermal perturbations.
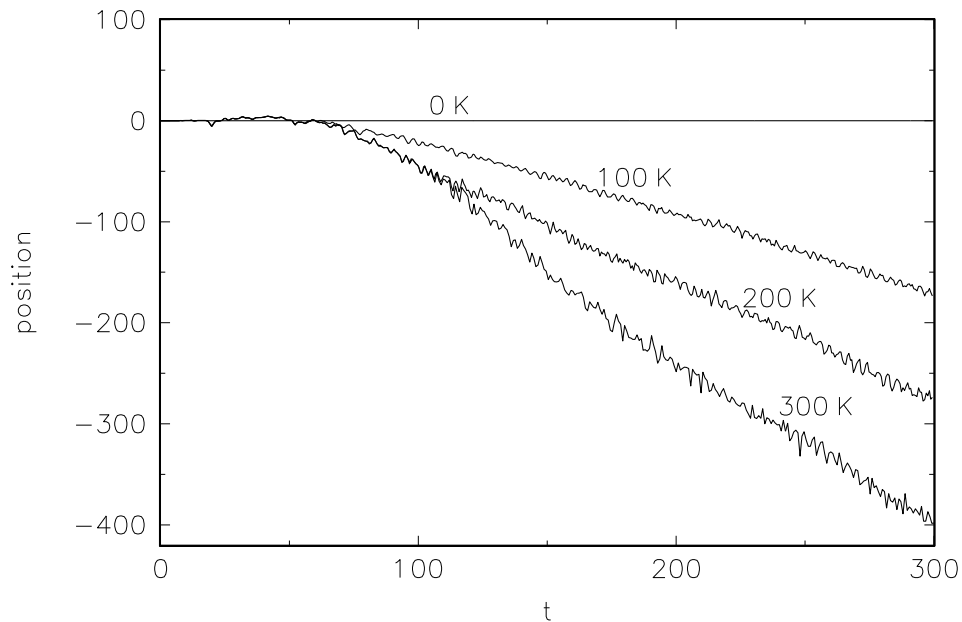
Acknowledgments

FIG. 23: Influence of temperature on the time-evolution of the breather center. Temperatures are indicated on the curves.

01183.

[1] J. Agarwal and D. Hennig. Breather solutions of a nonlinear DNA model including a longitudinal degree of freedom. *Physica A*, 323:519–533, 2003.
[2] GL Alfimov, VV Konotop, and M Salerno. Matter solitons in bose-einstein condensates with optical lattices. *Europhys. Lett.*, 58:7, 2002.
[3] A Álvarez, JFR Archilla, J Cuevas, and FR Romero. Dark breathers in Klein-Gordon lattices. Band analysis of their stability properties. *New Jornal of Physics*, 4:72, 2002.
[4] P W Anderson. Absence of diffusion in certain random lattices p w anderson. *Phys. Rev.*, 109:1492, 1958.
[5] JFR Archilla, PL Christiansen, and YuB Gaididei. Interplay of nonlinearity and geometry in a DNA–related, Klein–Gordon model with long–range dipole–dipole interaction. *Phys. Rev. E*, 65:016609, 2001.
[6] JFR Archilla, PL Christiansen, SF Mingaleev, and YuB Gaididei. Numerical study of breathers in a bent chain of oscillators with long range interaction. *J. Phys. A: Math. and Gen.*, 34:6363, 2001.
[7] JFR Archilla, YuB Gaididei, PL Christiansen, and J Cuevas. Stationary and moving breathers in a simplified model of curved alpha–helix proteins. *J. Phys. A: Math. and Gen.*, 35:8885, 2002.
[8] JFR Archilla, RS MacKay, and JL Marín. Discrete breathers and Anderson modes: two faces of the same phenomenon? *Physica D*, 134:406, 1999.
[9] T Asano et al. ESR investigation on the breather mode and the spinon-breather dynamical crossover in Cu benzoate. *Phys. Rev. Lett.*, 84:5880, 2000.
[10] S Aubry. Breathers in nonlinear lattices: Existence, linear stability and quantization. *Physica D*, 103:201, 1997.
[11] S Aubry and T Cretegny. Mobility and reactivity of discrete breathers. *Physica D*, 119:34, 1998.
[12] S. Aubry, G. Kopidakis, and V. Kadelburg. Variational proof for hard discrete breathers in some classes of Hamiltonian dynamical systems. *Discrete and Continuous Dynamical Systems*, 1:271, 2001.
[13] M. Barbi. *Localized Solutions in a Model of DNA Helicoidal Structure*. PhD thesis, Università degli Studi di Firenze, 1998.
[14] M. Barbi, S. Cocco, and M. Peyrard. Helicoidal model for DNA opening. *Phys. Lett. A*, 253(5–6):358–369, 1999.
[15] S.R. Bickham, S.A. Kiselev, and A.J. Sievers. Stationary and moving intrinsic localized modes in one-dimensional monatomic lattices with cubic and quartic anharmonicity. *Phys. Rev. B*, 47:14206, 1993.
[16] OM Braun and YuS Kivshar. Nonlinear dynamics of the Frenkel–Kontorova model. *Phys. Rep.*, 306:1, 1998.
[17] Ding Chen, S Aubry, and GP Tsironis. Breather mobility in discrete ϕ^4 lattices. *Phys. Rev. Lett.*, 77:4776, 1996.
[18] S. Cocco and R. Monasson. Statistical mechanics of torque induced denaturation of DNA. *Phys. Rev. Lett.*, 83(24):5178–5181, 1999.
[19] T Cretegny. *Dynamique collective et localisation de l'énergie dans les reseaux non-linaires*. PhD thesis, École Normale Supérieure de Lyon, 1998.
[20] J Cuevas. *Localization and energy transfer in anharmonic inhomogeneus lattices*. PhD thesis, University of Sevilla (Spain),

2003. In Spanish, http://www.us.es/gfnl/thesis.htm.

[21] J Cuevas, JFR Archilla, YuB Gaididei, and FR Romero. Moving breathers in a DNA model with competing short- and long-range dispersive interactions. *Physica D*, 163:106, 2002.

[22] J Cuevas, C Katerji, JFR Archilla, JC Eilbeck, and FM Russell. Influence of moving breathers on vacancies migration. *Phys. Lett. A*, 315:364–371, 2003.

[23] J Cuevas, F Palmero, JFR Archilla, and FR Romero. Moving breathers in a bent DNA model. *Phys. Lett. A*, 299:221, 2002.

[24] J Cuevas, F Palmero, JFR Archilla, and FR Romero. Moving discrete breathers in a Klein–Gordon chain with an impurity. *J. Phys. A: Math. and Gen.*, 35:10519, 2002.

[25] J Cuevas, EB Starikov, JFR Archilla, and D Hennig. Moving breathers in bent DNA with realistic parameters. *Modern Physics Letters B*, 18(25):1319, 2004.

[26] T. Dauxois, M. Peyrard, and A. R. Bishop. Dynamics and thermodynamics of a nonlinear model for DNA denaturation. *Phys. Rev. E*, 47(1):684–695, 1993.

[27] E. Delagoutte and P. H. von Hippel. Helicase mechanisms and the coupling of helicases within macromolecular machines Part ii: Integration of helicases into cellular processes. *Q. Rev. of Biophys.*, 36(1):1–69, 2003.

[28] J Dorignac, JC Eilbeck, M Salerno, and A C Scott. Quantum signatures of breather-breather interactions. *Phys. Rev. Letts.*, 93:025504, 2004.

[29] J C Eilbeck and F Palmero. Quantum breathers in an attractive Fermionic Hubbard model. In F Kh Abdullaev and V V Konotop, editors, *Nonlinear Waves: Classical and Quantum Aspects*, pages 399–412, Amsterdam, 2004. Kluwer.

[30] J C Eilbeck and F Palmero. Trapping in quantum chains. *Phys. Lett. A*, 331:201, 2004.

[31] JC Eilbeck. *Computer Analysis for Life Science*. C Kawabata and AR Bishop, 12 Ohmsha: Tokyo, 1986.

[32] S. W. Englander, N. R. Kallenbach, A. J. Heeger, J. A. Krumhansl, and S. Litwin. Nature of the open state in long polynucleotide double helices: Possibility of soliton excitations. In *Proc. Natl. Acad. Sci. USA*, volume 77, pages 7222–7226, 1980.

[33] F Fillaux, C J Carlile, and G J Kearley. Inelastic-neutron-scattering study of the sine-Gordon breather interactions in isotopic mixtures of 4-methyl-pyridine. *Phys. Rev. B*, 58:11416, 1998.

[34] S. Flach and A. Gorbach. Discrete breathers in Fermi-Pasta-Ulam lattices. *CHAOS*, 15:015112, 2005.

[35] YuB Gaididei, SF Mingaleev, PL Christiansen, and KØ Rasmussen. Effects of nonlocal dispersive interactions on self-trapping excitations. *Phys. Rev. E*, 55:6141–6150, 1997.

[36] D Hennig. Control of electron transfer in disordered DNA under the impact of viscous damping and an external periodic field. *Eur. Phys. J. B*, 30:211, 2002.

[37] D Hennig, JFR Archilla, and J Agarwal. Nonlinear charge transport mechanism in periodic and disordered DNA. *Physica D*, 180:256, 2003.

[38] D Hennig, EB Starikov, JFR Archilla, and F Palmero. Moving breathers in bent DNA with realistic parameters. *Journal of Biological Physics*, 30:227, 2004.

[39] P Jakob. Anharmonic coupling effects among adsorbate vibrational modes: The model system Ru(001)- $\sqrt{3} \times \sqrt{3}$ R30-CO revisited. *Appl. Phys. A*, 75(45), 2002.

[40] G. James. Existence of breathers on FPU lattices. *C. R. Acad. Sci. Paris*, 332:581–586, 2001.

[41] G. James. Centre manifold reduction for quasilinear discrete systems. *J. Nonlinear Sci.*, 13:27, 2003.

[42] G Kalosakas, S Aubry, and GP Tsironis. Polaron solutions and normal–mode analysis in the semiclassical Holstein model. *Phys. Rev. B*, 58:3094–3104, 1998.

[43] M. Kastner. Energy thresholds for discrete breathers. *Phys. Rev. Lett.*, 92:104301, 2004.

[44] H-Y Lee et al. Control of electrical conduction in DNA using oxygen hole doping. *Appl. Phys. Lett*, 80:1670, 2002.

[45] Xiaoqin Li et al. An all-optical quantum gate in a semiconductor quantum dot. *Science*, 301:809, 2003.

[46] RS MacKay and S Aubry. Proof of existence of breathers for time-reversible or Hamiltonian networks of weakly coupled oscillators. *Nonlinearity*, 7:1623, 1994.

[47] JL Marín. *Intrinsic Localized Modes in nonlinear lattices*. PhD thesis, University of Zaragoza (Spain), June 1997.

[48] JL Marín and S Aubry. Breathers in nonlinear lattices: Numerical calculation from the anticontinuous limit. *Nonlinearity*, 9:1501, 1996.

[49] JL Marín and S Aubry. Finite size effects on instabilities of discrete breathers. *Physica D*, 119:163, 1998.

[50] JL Marín, S Aubry, and LM Floría. Intrinsic localized modes: Discrete breathers. existence and linear stability. *Physica D*, 113:283, 1998.

[51] SF Mingaleev, PL Christiansen, YuB Gaididei, M Johansson, and KØ Rasmussen. Models for energy and charge transport and storage in biomolecules. *J. Biol. Phys.*, 25:41, 1999.

[52] F Palmero, JFR Archilla, D hennig, and FR Romero. Effect of base-pair inhomogeneities on charge transport along the DNA molecule, mediated by twist and radial polarons. *New Journal of Physics*, 6:13, 2004.

[53] M Peyrard and AR Bishop. Statistical mechanics of a nonlinear model for DNA denaturation. *Phys. Rev. Lett.*, 62:2755, 1989.

[54] D Porath, A Bezryadin, S de Vries, and C. Dekker. Direct measurements of electrical transport through DNA molecules. *Nature*, 403:635, 2000.

[55] K.W. Sandusky and J.B. Page. Interrelation between the stability of extended normal modes and the existence of intrinsic localized modes in nonlinear lattices with realistic potentials. *Phys. Rev. B*, 50:866, 1994.

[56] L S Schulman et al. Slow relaxation, confinement, and solitons. *Phys. Rev. Lett.*, 88:224101, 2002.

[57] A C Scott. *Nonlinear Science*. OUP, Oxford, 1999.

[58] A C Scott, J C Eilbeck, and H Gilhøj. Quantum lattice solitons. *Physica D*, 78:194, 1994.

[59] A.J. Sievers and S. Takeno. Intrinsic localized modes in anharmonic crystals. *Phys. Rev. Lett.*, 61:970, 1988.

[60] B. Snchez-Rey, G. James, J. Cuevas, and JFR Archilla. Bright and dark breathers in Fermi-Pasta-Ulam lattices. *Phys. Rev. B*, 70:014301, 2004.

[61] L Stryer. *Biochemistry*. Freeman, New York, 1995.

[62] P. H. von Hippel and E. Delagoutte. A general model for nucleic acid helicases and their "coupling" within macromolecular machines. *Cell*, 104(2):117–190, 2001.

[63] L. Wu and I. D. Hickson. DNA ends recQ-uire attention. *Science*, 292:229–230, 2001.